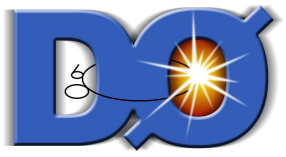

DØ Note 6346-CONF

Updated search for Higgs boson production in final states with a lepton, missing energy, and at least two jets in 9.7 fb^{-1} of Tevatron data

The DØ Collaboration
URL http://www-d0.fnal.gov
(Dated: July 3, 2012)

We present a search for the Higgs boson in final states with a charged lepton (electron or muon), missing energy, and two or more jets corresponding to 9.7 fb^{-1} of integrated luminosity collected with the D0 detector at the Fermilab Tevatron $p\bar{p}$ collider. The search is sensitive to $WH \to \ell\nu b\bar{b}$, $(gg, VV) \to H \to WW \to \ell\nu jj$ (where $j = u, d, s$ or g) and $VH \to VWW \to \ell\nu jjjj$ production (where $V = W$ or Z). We observe good agreement between data and expected background. For $M_H = 125$ GeV we set a 95% C.L. upper limit on the production of a standard model Higgs boson of $4.5\times\sigma_{SM}$, where σ_{SM} is the standard model cross section, while the expected limit is $4.1\times\sigma_{SM}$.

Preliminary Results for the 2012 Summer Conferences

I. INTRODUCTION

The only unobserved fundamental particle in the standard model (SM) is the Higgs boson, predicted as a consequence of describing spontaneous electroweak symmetry breaking using the Higgs mechanism. Its observation would confirm the hypothesis that the Higgs mechanism generates the masses of the weak gauge bosons and also provide an explanation for the finite masses of fermions via their Yukawa couplings to the Higgs field. The mass of the Higgs boson (M_H) is a free parameter in the SM, but it is constrained by experiment. The direct searches at the CERN e^+e^- Collider (LEP) [1] exclude $M_H < 114.4$ GeV at the 95% C.L. and precision measurements of other electroweak parameters constrain M_H to be less than 152 GeV at the 95% C.L [2–4]. The M_H region 147–179 GeV is excluded at the 95% C.L. by the CDF and D0 combined analysis [5]. ATLAS and CMS at the Large Hadron Collider (LHC) have excluded M_H values 110.0–117.5 GeV, 118.5–122.5 GeV, and 129–539 GeV (ATLAS) [6] and 127.5–600 GeV (CMS) [7] at the 95% C.L. The remaining allowed mass range is being probed further at the Fermilab Tevatron Collider. This paper describes searches for the SM Higgs boson in events with a charged lepton (electron or muon), missing energy, and two or more jets in the final state.

The dominant process for Higgs boson production at the Tevatron is gluon fusion, but additional production mechanisms, including associated production of a Higgs boson and a W or a Z boson and direct production via vector boson fusion, occur at rates reduced by roughly an order of magnitude. At masses below $M_H \approx 135$ GeV, the branching fraction of $H \to b\bar{b}$ dominates, while $H \to WW$ is the favored decay channel above 135 GeV. In the low mass region, associated production of a Higgs boson and a W boson is one of the most sensitive search channels at the Tevatron. Maximizing the sensitivity of the SM Higgs boson search also requires all channels to be exploited and combined. Studying final states with a lepton, missing energy, and two or more jets in the final state is sensitive to $WH \to \ell\nu b\bar{b}$, $(gg, VV) \to H \to \ell\nu jj$, and $VH \to VWW \to \ell\nu jjjj$ production ($V = W$ or Z). The analysis is optimized for these production and decay mechanisms by organizing events into subchannels based on jet multiplicity and the number and quality of candidate b-quark jets.

Several searches for $WH \to \ell\nu b\bar{b}$ production have already been published at a $p\bar{p}$ center-of-mass energy of $\sqrt{s} = 1.96$ TeV. Four of these [8–11] use subsamples (0.17 fb^{-1}, 0.44 fb^{-1}, 1.1 fb^{-1} and 5.3 fb^{-1}) of the data analyzed in this paper. A previous search in the $H \to WW \to \ell\nu jj$ channel at D0 uses a 5.4 fb^{-1} subsample of the data used in this paper [12, 13].

We present an updated search using a multivariate approach with a data sample of 9.7 fb^{-1} collected by the D0 experiment. The search is based on events with one charged lepton ($\ell = e$ or μ), an imbalance in transverse energy ($\not\!\!E_T$) that arises from the neutrino in the $W \to \ell\nu$ decay, and two or more jets, with zero or more of these jets selected as candidate b-quark jets (b-tagged). Major updates to this analysis since March, 2012 [14], and the changes in our results due to these updates are described in detail in Appendix B.

We use the output of a multivariate b-jet identifier to classify events based on the number b-tagged jets and their b-ID discriminant outputs. Each b-tag category has a different composition of background contributions from SM processes. The dominant backgrounds in zero-b-tagged events are from W boson production in association with light-quark jets and multijet events where a jet is misidentified as an isolated lepton. Single-b-tagged events contain three important sources of backgrounds: (i) W boson production in association with light-quark jets and possibly one c-quark jet, (ii) W boson production in association with two jets emerging from heavy flavor quarks ($b\bar{b}, c\bar{c}$; "heavy-flavor" jets), and (iii) multijet events. In events with two b-tagged jets, the dominant backgrounds are from $Wb\bar{b}$ and $t\bar{t}$.

We use a Boosted Decision Tree (BDT) multivariate analysis technique [15] to separate the SM background from signal in the selected events and search for an excess of data consistent with the signal. Signal-like events tend to have larger BDT discriminant output values than background-like events. This multivariate technique combines a number of variables with mild discrimination power between signal and background into a more powerful signal discriminant. The input variables used for each multivariate in this analysis are described in detail in Appendix A. In events with exactly 2 or 3 jets, only events with one or more b-tagged jets are considered in this search. In events with four or more jets, only events with zero or one b-tagged jet are considered in this search. A separate BDT discriminant is created for each considered combination of final state jet multiplicity, lepton flavor (e or μ), and b-tagged jet category.

This analysis uses most of the major components of the D0 detector [16]. The central-tracking system consists of a silicon microstrip tracker (SMT) and a central fiber tracker (CFT) located within a 2 T superconducting solenoidal magnet. Central and forward preshower detectors are located just outside of the superconducting coil. The liquid-argon sampling calorimeter consists of a central section (CC), covering pseudorapidity $|\eta| < 1.1$ relative to the center of the detector [17] and two end calorimeters (EC) extending coverage to $|\eta| < 4.2$. These three calorimeters are housed in separate cryostats [18], with scintillators between the CC and EC cryostats providing additional sampling of developing showers at $1.1 < |\eta| < 1.4$. The muon system is located beyond the calorimetry and consists of layers of tracking detectors and scintillation trigger counters before and after 1.8 T iron toroidal magnets. In 2006 the detector was upgraded to add an additional layer of silicon to the SMT [19] and an improved calorimeter trigger [20], and the installation of improved tracking electronics was completed in 2007.

The luminosity is measured using plastic scintillator arrays located in front of the EC cryostats at $2.7 < |\eta| < 4.4$. We reject data in which the tracking, calorimeter, or muon information may have been compromised. The trigger and data acquisition systems are designed to accommodate the high instantaneous luminosities of Run II.

Events in the electron channel are triggered by a logical OR of several triggers requiring an electromagnetic (EM) object with or without additional jets. This trigger combination is $\sim 95\%$ efficient for selecting electron channel signal events within our acceptance. Trigger efficiencies are taken into account in the simulation through a reweighting of events, based on an efficiency derived from data, and parametrized as a function of electron η, azimuth ϕ, and jet p_T.

We accept events containing a muon from an inclusive mixture of single muon, muon plus jet, $\not\!\!E_T$ plus jet, and multijet triggers. The MC events are first reweighted to correct the efficiency for events to be triggered by a subset of single muon and muon plus jet triggers. Including the additional triggers provides approximately a 30% increase in efficiency over only using the single muon and muon plus jet trigger subset. The additional correction of this complementary set of triggers is modeled as a function of the scalar sum of jet p_T (H_T), muon η and muon ϕ. An additional event weight adjustment is applied to each MC event based on this correction in order to model the inclusive mixture of triggers. We observe good agreement between data and MC when combining all the triggers to form the inclusive dataset.

II. SIMULATED DATASETS

Simulation of background and signal processes relies on the CTEQ6L1 [21, 22] leading-order parton distribution functions for all MC event generators. The V+jets and $t\bar{t}$ events are generated with `ALPGEN` [23] interfaced to `PYTHIA` [24] for parton showering and hadronization. `ALPGEN` samples are produced using the MLM parton-jet matching prescription [23]. The V+jets samples contain Vjj and Vcj processes, while $Vb\bar{b}$ and $Vc\bar{c}$ are generated separately. The `PYTHIA` [24] MC generator is used to simulate the production of dibosons with inclusive decays (WW, WZ and ZZ), and all signal processes. Single top-quark events are generated with the `SingleTop` event generator [25, 26] and use `PYTHIA` for parton evolution and hadronization. All generated events are processed through a full D0 detector simulation (based on `GEANT` [27]), using the same reconstruction software as is used for D0 data. Data events from random beam crossings are overlaid to account for multiple $p\bar{p}$ interactions.

The simulated background cross sections are normalized to the SM predictions, except for V+jets events, which are normalized to data before applying b-tagging, where the contamination from signal is predicted to be negligible. The predicted signal cross sections are taken from Ref. [28]. NLO cross sections are used for $t\bar{t}$ (approximate NNLO) [29], single-top [30], and diboson [31, 32]. As a cross check, we compare data with the `ALPGEN` prediction for V+jets, corrected in such a way that the inclusive W production cross section is equal to its NNLO calculation [33–35] with MSTW2008 NNLO PDFs [36], and we find a relative data/MC normalization factor of 1.0 ± 0.1 for V+jets, where the normalization factor from data is obtained after subtracting all other expected background processes. The V+heavy-flavor jet events simulated by `ALPGEN` are corrected by the LO to NLO ratio obtained from `MCFM` [32, 37] separately for $Vb\bar{b}$, $Vc\bar{c}$, and V+light jets processes.

III. EVENT SELECTION

This analysis is based on the selection of events with exactly one electron with $p_T > 15$ GeV and $|\eta| < 1.1$ or $1.5 < |\eta| < 2.5$, or exactly one muon with $p_T > 15$ GeV and $|\eta| < 2.0$. Events are also required to have $\not\!\!E_T > 15$ (20) GeV for the electron (muon) channel, and two or more jets with $p_T > 20$ GeV (after calibration of the jet energy [38]) and $|\eta| < 2.5$. $\not\!\!E_T$ is calculated from the individual calorimeter cells, ignoring unclustered energy in cells of the outermost readout layers of the calorimeter, and is corrected for the presence of any muons.

Events with additional charged leptons, isolated from jets, that pass a flavor-dependent p_T threshold ($p_T^e > 20$ GeV, $p_T^\mu > 15$ GeV and $p_T^\tau > 10$ or 15 GeV for hadronically decaying τ leptons; τ lepton identification is described in [39]) are rejected to suppress dilepton backgrounds from Z, $t\bar{t}$, and WW events. Only events with a primary vertex (with at least three tracks) located within ± 60 cm of the nominal longitudinal interaction point, measured along the proton beam axis, are selected for further analysis.

Lepton candidates are identified in two steps, in a similar manner to that described in [13]: (i) each candidate must pass "loose" identification criteria. For electrons, we require a loose cut on a multivariate discriminator that makes use of inputs that include: ratio of calorimeter energy to track momentum; fraction of total energy in a shower that is deposited in the EM section of the calorimeter; calorimeter isolation fraction (ratio of the EM energy in a $\Delta\mathcal{R} < 0.2$ cone in the (η, ϕ) space [17] to the total calorimeter energy in a $\Delta\mathcal{R} < 0.4$ cone around the electron); calorimeter shower shape information; track match probability; track isolation information; track hits in the SMT and the CFT; tracker activity in the projected electron road; and central preshower hit information. For a loose

muon, we require the timing of scintillator hits to coincide with a beam crossing, a match of the reconstructed track in the muon system with one in the central tracker, and isolation from jets to reject muons from semileptonic decay of hadrons ($\Delta\mathcal{R} > 0.5$). (ii) The loose leptons then undergo a final "tight" selection. Tight electrons must satisfy a more restrictive cut on the multivariate electron identifier. Tight muons must satisfy stricter isolation criteria on energy in the calorimeter and momenta of tracks near the trajectory of the muon candidate. Inefficiencies introduced by lepton-identification and isolation criteria are determined from $Z \to \ell\ell$ data and used to correct the efficiency in simulated events to match that in the data. The final selections rely only on tight leptons, with loose leptons used to determine the multijet background.

IV. MULTIJET MODELING AND W+JETS NORMALIZATION

Instrumental backgrounds and those from semi-leptonic decays of hadrons, referred to jointly as the multijet background, are estimated from data. The instrumental background is important for the electron channel, where a jet with high EM fraction can pass electron identification criteria, or a photon can be misidentified as an electron. In the muon channel, the multijet background is less significant, and arises mainly from the semi-leptonic decay of heavy quarks, where the muon satisfies the isolation requirements.

The multijet background is estimated in each channel based on events in data that pass the loose but fail the tight lepton identification criteria (i.e. "loose-not-tight" events). We first determine the probability, $f_{T|L}$, for a jet that passes loose electron criteria to pass tight electron criteria. This is done in events that pass preselection requirements, i.e., they contain one loose lepton and two jets, but with small $\not\!\!E_T$, i.e. $5 < \not\!\!E_T < 15$ GeV. The total non-multijet background present with this selection is estimated from MC and subtracted from the data to estimate the contribution from multijet events. The probability $f_{T|L}$ is defined by the ratio of the estimated multijet yield including only tight leptons to that containing loose and tight leptons. For electrons, $f_{T|L}$ is determined as a function of electron p_T in three regions of $|\eta|$ and in four regions of $\Delta\phi(\not\!\!E_T, e)$. For muons, $f_{T|L}$ is determined as a function of muon p_T, muon detector η, and $\Delta\phi(\not\!\!E_T, \mu)$. Each loose-not-tight event is assigned a weight that contributes to the multijet estimation based on $f_{T|L}$ as a function of event kinematics. Since $f_{T|L}$ depends on $\not\!\!E_T$, the scale of this estimate of the multijet background must be adjusted when comparing to data with $\not\!\!E_T >$ 15 (20) GeV for electron (muon) channels. Before applying b-tagging, we perform a fit to the transverse mass of the W candidate (M_W^T) distribution in both channels to set the scale of the multijet and W/Z+jets backgrounds simultaneously. The V+jets MC estimates are reduced in order to compensate for the contamination of events with real leptons in this multijet estimate. To suppress multijet background, events with $M_W^T < 40$ GeV $- 0.5\ \not\!\!E_T$ GeV are removed in both the electron and muon channels.

To further suppress the multijet background, we develop a multivariate technique (MVAQCD) that exploits kinematic differences between the multijet background and signal. The MVAQCD is a Boosted Decision Tree (BDT) developed with the TMVA package [40]. It employs 12 variables that separate the signal from the multijet background and show good agreement between the data and background estimates in the preselection sample. A full description of these input variables appears in Tab. V in Appendix A. For training we use $WH \to \ell\nu b\bar{b}$ events as a signal, and combine three Higgs boson mass points: 120, 125 and 130 GeV. We verify that that the output distribution is well-modeled after preselection, as shown in Fig. 1.

V. JET MODELING CORRECTIONS

Jets are reconstructed using a midpoint cone algorithm [41] with a radius of $\Delta\mathcal{R} = \sqrt{(\Delta y)^2 + (\Delta\phi)^2} = 0.5$, where y is the jet rapidity. Identification requirements ensure that the distribution in jet energy for all layers of the calorimeter is reasonable and that jets are not caused by noise or spurious depositions of energy. The difference in efficiency for jet identification and jet resolution between data and simulation is taken into account in the overall MC correction for jet reconstruction efficiency and energy resolution. Comparison of `ALPGEN` with other generators [42] and with data shows discrepancies in distributions of jet pseudorapidity and dijet angular separations. The data are therefore used to correct the `ALPGEN` W+jets and Z+jets MC events by reweighting the simulated lepton η distribution, the leading and second-leading jet η distributions, the $\Delta\mathcal{R}$ distribution between the two leading jets, and W boson p_T in the W/Z+jets samples through the use of polynomial functions that bring the total simulated background into agreement with the high statistics pre-b-tagged data. After this step, the jet distributions in simulations are in agreement with the data over the complete range of kinematics.

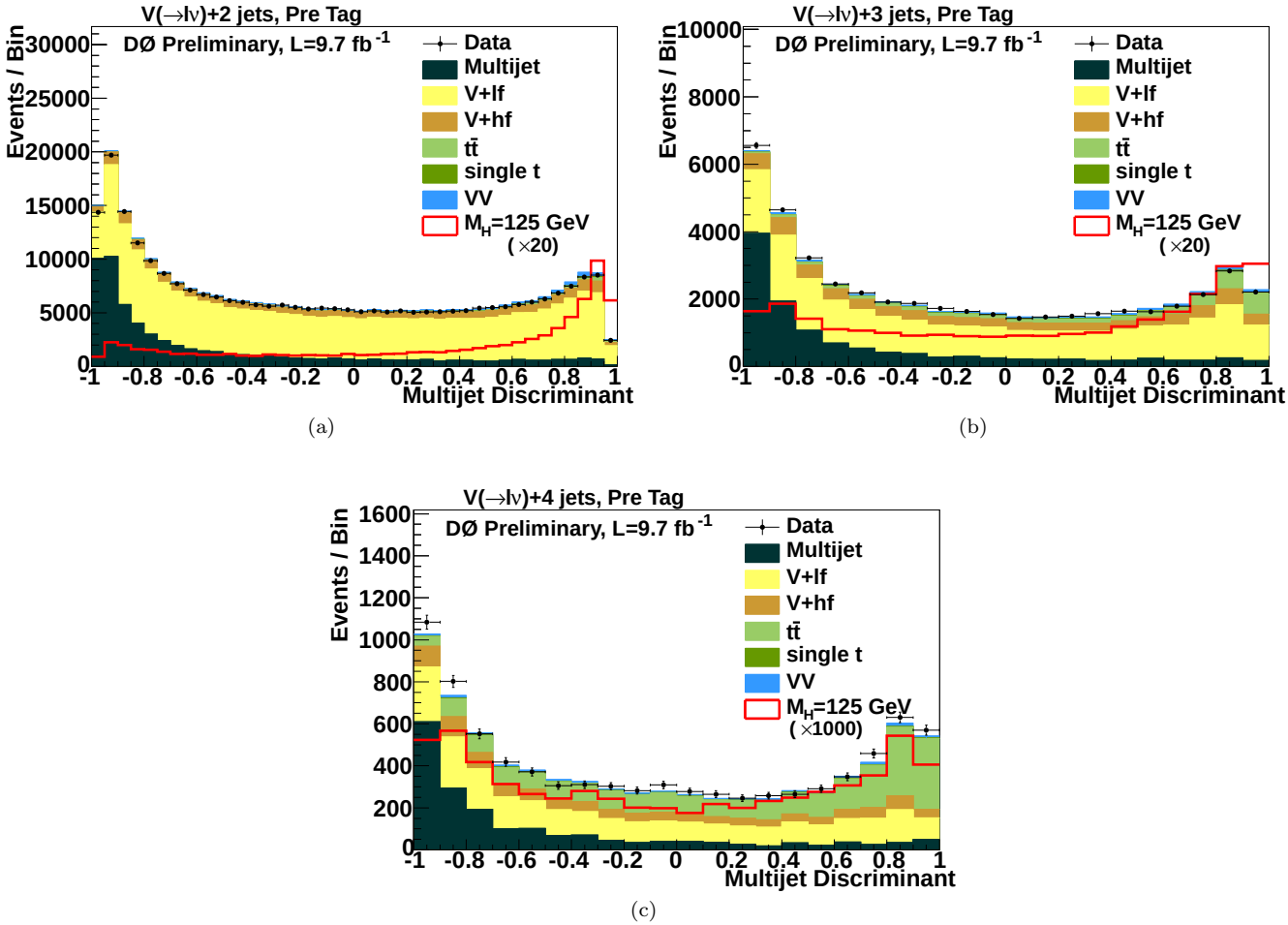

FIG. 1: Multivariate multijet discriminant output for all Run II electron and muon channels before b-tagging in (a) 2-jet, (b) 3-jet, and (c) 4-jet events. Signal events are scaled by a factor of 1000. The signal shown is for a Higgs mass of 125 GeV.

VI. EVENT YIELDS AND MULTIVARIATE DISCRIMINANTS

Efficient identification of b-jets is central to the search for WH production. The D0 b-tagging algorithm for identifying heavy-flavored jets is based on a combination of variables sensitive to the presence of tracks or secondary vertices displaced significantly from the primary vertex. This algorithm makes use of a BDT and provides improved performance over the previous Neural Network based algorithm that is described in Ref. [43]. The efficiency is determined for taggable jets, where taggable jets have at least two tracks of good quality with at least one hit in the SMT. Simulated events are corrected to have the same fraction of jets satisfying the taggability and b-tagging requirements as found in preselected data.

Cuts on the continuous b-ID BDT output are used to define the tagging categories. The zero b-tags category includes all events where none of the selected jets are taggable. Events with exactly one b-tagged jet are assigned to the one tight b-tag category if the b-ID discriminant output is high enough to pass the selection threshold and to the one loose b-tag category otherwise. Events with two or more b-tagged jets are assigned to either the two loose b-tags, two medium b-tags, or two tight b-tags category, depending on the average b-ID discriminant value of the two highest b-tagged jets. The operating point for the loose threshold has an identification efficiency of 79% for individual b-jets, averaged over our selected jet p_T and η distributions, with a b-tagging misidentification rate of $\approx 11\%$ for light-quark jets. The medium threshold has an efficiency of 57% for individual b-jets and a b-tagging misidentification rate of 0.6% for light-quark jets. The tight b-tag threshold has an efficiency of 47% for individual b-jets and a b-tagging misidentification rate of 0.15% for light-quark jets.

After applying these selection criteria, the expected event yields for the backgrounds and for a sample Higgs boson mass ($M_H = 125$ GeV) are compared to the observed number of events in 2-jet, 3-jet and 4-jet events in Tables I, II,

and III, respectively. Distributions of the dijet invariant mass, using the two jets of highest b-ID output (or highest p_T jets if fewer than two b-tagged jets are available), in W+2-jets, W+3-jets, and W+4-jets events before dividing into b-tag categories are shown in Fig. 2. The same distribution is shown for each combination of jet multiplicity and b-tag category in Figures 3, 4, and 5. The data are well described by the predicted background. The contributions expected from a Higgs boson with $M_H = 125$ GeV are shown. The total signal contribution from $H \to b\bar{b}$ decay channels decreases as M_H increases, while the total signal contribution from $H \to WW$ decay channels has the opposite trend. At $M_H \approx 130$ GeV and higher, the $H \to WW$ decay channels begin to make significant contributions to the search sensitivity.

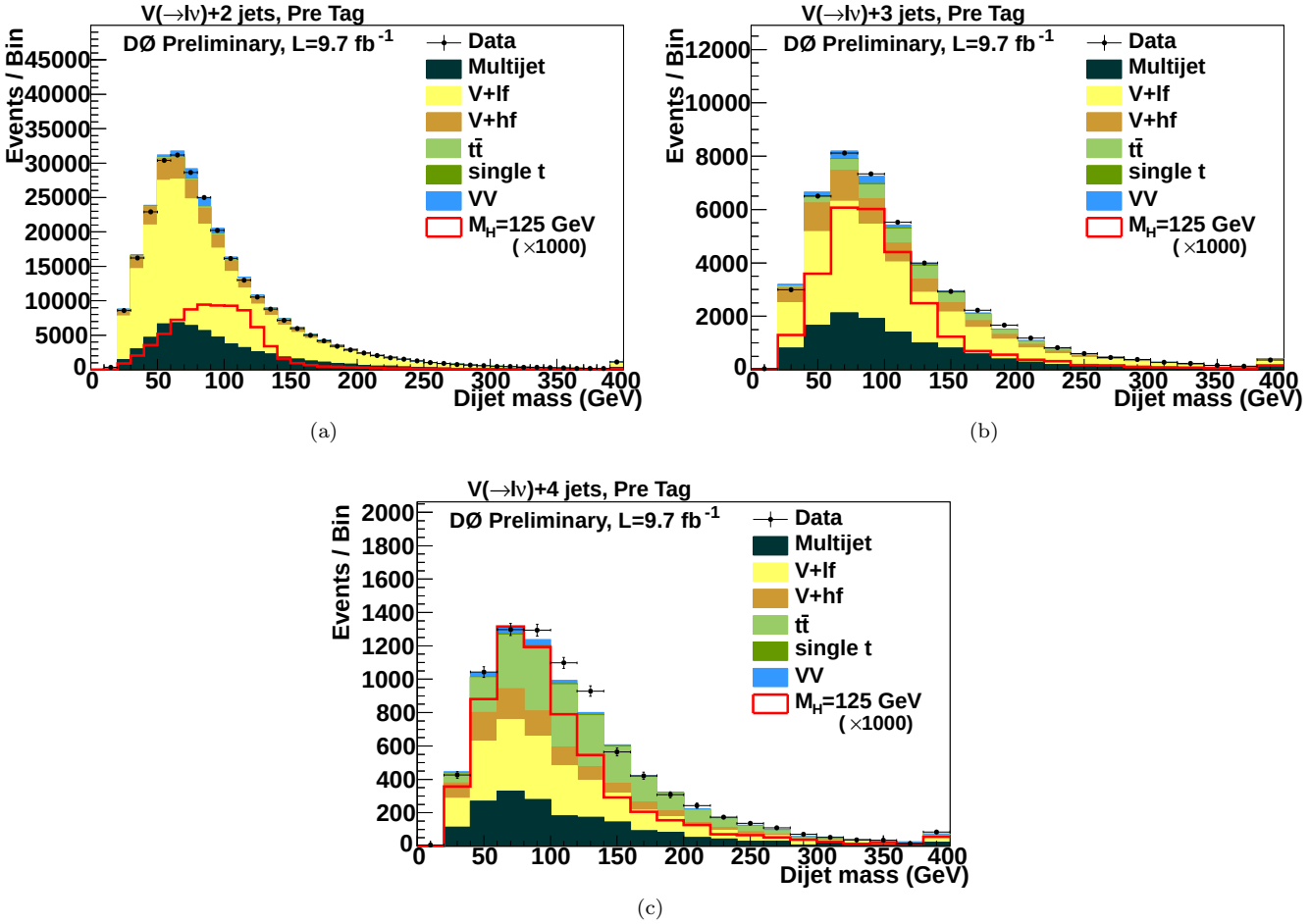

FIG. 2: Dijet mass distribution for all Run II electron and muon channels, prior to division into b-tagging categories, in (a) 2-jet, (b) 3-jet, and (c) 4-jet events. Signal events are scaled by a factor of 1000. The signal shown is for a Higgs mass of 125 GeV.

To further separate signal and background we use a BDT trained on the Higgs samples, VH in a case of the 2 and 3 jets, and the combined processes in a case of the 4 jets, as signal and all the SM processes as background. An independent BDT is created for each channel using a channel-optimized set of inputs. A full list of the input variables for each channel can be found in Tabs. VI-VII in Appendix A. drawn from such variables as b-ID information, MVAQCD output, particle 4-vectors, angles between objects, and combinations of kinematic variables such as reconstructed masses and event shapes. When selecting input variables we ensure that each is well-modeled and displays good separation between signal and one or more backgrounds. We train a separate BDT for each Higgs mass considered, with M_H varying between 100–200 GeV in 5 GeV steps, for each of the independent analysis channels. All channels are considered simultaneously when performing our limit calculations. Figures 6, 7, and 8 show the BDT output distributions for all 2-jet, 3-jet, and 4-jet event channels, respectively.

TABLE I: Summary of event yields for the ℓ + 2 jets + $\not\!\!E_T$ final states in Run II data. Events in data are compared with the expected number of events in the W/Z+jets samples, in simulated samples of diboson (including WW, WZ, and ZZ processes), $W/Z+b\bar{b}$ or $c\bar{c}$, W/Z+light-quark jets, top quark ("$t\bar{t}$" and "Single top") production, and the multijet background derived from data. All signal yields are for $M_H = 125$ GeV. Events with 0 and 1 loose b-tags are not used in this channel. Uncertainties include only the contribution from statistics.

	pre-b-tagging	0 b-tags	1 loose b-tag	1 tight b-tag	2 loose b-tags	2 medium b-tags	2 tight b-tags
$WH\to\ell\nu b\bar{b}$	33.70±0.12	5.64±0.04	3.61±0.03	10.49±0.08	2.84±0.04	4.17±0.05	7.05±0.07
$ZH\to\ell b\bar{b}+\not\!\!E_T$	3.57±0.02	0.71±< 0.01	0.40±< 0.01	1.11±0.01	0.31±< 0.01	0.44±0.01	0.68±0.01
$gg\to H\to WW\to\ell\nu jj$	21.03±0.19	16.00±0.17	3.28±0.07	1.59±0.04	0.27±0.02	0.07±0.01	< 0.01±< 0.01
$gg\to H\to ZZ\to\ell\ell jj$	0.36±< 0.01	0.27±< 0.01	0.05±< 0.01	0.03±< 0.01	< 0.01±< 0.01	< 0.01±< 0.01	< 0.01±< 0.01
$VV\to H\to WW\to\ell\nu jj$	3.34±0.03	2.52±0.03	0.57±0.01	0.21±< 0.01	0.04±< 0.01	< 0.01±< 0.01	< 0.01±< 0.01
$VH\to VWW\to\ell\nu+4j$	12.96±0.12	9.34±0.11	2.25±0.05	1.19±0.04	0.26±0.02	0.04±< 0.01	0.01±< 0.01
Diboson	5686.2±10.7	4034.5±9.3	968.2±4.4	535.2±3.1	109.3±1.4	42.3±0.8	38.0±0.6
$W+b\bar{b}$	7396.9±16.2	2433.8±9.4	1101.4±6.5	2495.6±9.3	375.5±3.8	448.9±4.0	568.8±4.3
$Z+b\bar{b}$	716.3±1.6	252.8±1.0	108.6±0.7	249.1±0.9	33.6±0.4	39.5±0.4	45.3±0.4
$W+c\bar{c}$	17712.0±32.1	11349.1±26.2	3354.0±13.9	2282.2±11.1	522.4±5.2	185.1±2.9	71.0±1.8
$Z+c\bar{c}$	1617.4±4.1	1053.5±3.4	308.0±1.8	209.2±1.4	46.7±0.7	17.1±0.4	6.3±0.2
$t\bar{t}$	2378.7±4.0	502.3±2.2	299.8±1.6	822.4±2.5	180.7±1.1	245.1±1.2	346.9±1.3
Single top	1149.2±2.0	256.2±1.1	154.5±0.8	467.3±1.4	66.0±0.5	87.9±0.5	115.3±0.5
Multijet	58001.8±161.7	43545.5±139.7	9316.3±65.8	3700.1±41.1	946.4±21.4	298.3±11.7	195.3±9.1
$W+(u,d,s)$-jets	170013.1±159.8	138246.6±146.5	24722.6±61.0	5841.0±29.2	1654.7±15.8	125.4±4.4	12.8±1.4
$Z+(u,d,s)$-jets	12258.2±26.9	10439.6±25.2	1698.2±10.2	332.7±4.2	107.7±2.4	6.1±0.6	0.4±0.2
Total expectation	276929.7±232.1	212113.8±206.1	42031.5±91.8	16934.7±27.6	4042.9±206.1	1495.6±13.5	1400.3±10.2
Observed Events	276929	211169	42774	16406	4057	1358	1165

TABLE II: Summary of event yields for the ℓ + 3 jets + $\not\!\!E_T$ final states in Run II data. Events in data are compared with the expected number of events in the W/Z+jets samples, in simulated samples of diboson (including WW, WZ, and ZZ processes), $W/Z+b\bar{b}$ or $c\bar{c}$, W/Z+light-quark jets, top quark ("$t\bar{t}$" and "Single top") production, and the multijet background derived from data. All signal yields are for $M_H = 125$ GeV. Events with 0 and 1 loose b-tags are not used in this channel. Uncertainties include only the contribution from statistics.

	pre-b-tagging	0 b-tags	1 loose b-tag	1 tight b-tag	2 loose b-tags	2 medium b-tags	2 tight b-tags
$WH\to\ell\nu b\bar{b}$	7.50±0.05	1.11±0.02	0.83±0.02	2.05±0.03	0.78±0.02	0.94±0.03	1.48±0.03
$ZH\to\ell b\bar{b}+\not\!\!E_T$	1.13±0.01	0.18±< 0.01	0.13±< 0.01	0.33±< 0.01	0.12±< 0.01	0.15±< 0.01	0.20±< 0.01
$gg\to H\to WW\to\ell\nu jj$	5.56±0.09	3.89±0.09	1.04±0.04	0.53±0.03	0.16±0.02	0.05±< 0.01	0.01±< 0.01
$gg\to H\to ZZ\to\ell\ell jj$	0.13±< 0.01	0.07±< 0.01	0.01±< 0.01	0.01±< 0.01	< 0.01±< 0.01	< 0.01±< 0.01	< 0.01±< 0.01
$VV\to H\to WW\to\ell\nu jj$	3.07±0.03	2.06±0.03	0.66±0.01	0.26±0.01	0.10±< 0.01	0.02±< 0.01	< 0.01±< 0.01
$VH\to VWW\to\ell\nu+4j$	7.26±0.09	4.50±0.07	1.61±0.05	0.86±0.03	0.32±0.02	0.05±< 0.01	0.01±< 0.01
Diboson	1138.0±4.8	726.5±4.0	238.0±2.2	112.8±1.4	42.2±0.9	14.4±0.5	9.9±0.3
$W+b\bar{b}$	1610.6±7.6	457.2±4.2	249.6±3.1	512.1±4.3	122.0±2.2	125.3±2.1	119.6±2.0
$Z+b\bar{b}$	203.4±0.9	57.5±0.5	32.1±0.4	67.9±0.5	15.3±0.3	16.3±0.3	16.2±0.2
$W+c\bar{c}$	4333.2±16.4	2423.2±12.6	961.4±7.8	600.3±5.9	246.2±3.8	77.6±2.1	25.7±1.1
$Z+c\bar{c}$	478.2±2.4	275.0±1.9	106.3±1.1	69.8±0.9	27.6±0.6	8.9±0.3	2.7±0.1
$t\bar{t}$	3383.7±6.2	510.9±2.6	382.4±2.3	1020.9±3.5	337.9±2.1	425.0±2.2	525.3±2.2
Single top	310.5±1.1	51.9±0.5	37.0±0.4	102.3±0.7	27.2±0.3	34.9±0.3	45.2±0.4
Multijet	10364.1±70.2	6629.0±56.8	2162.4±32.7	933.4±20.4	367.4±12.6	130.4±7.4	82.1±4.9
$W+(u,d,s)$-jets	21908.1±51.4	16363.9±46.0	4171.2±22.4	900.2±10.0	533.4±8.0	31.6±1.9	3.1±1.1
$Z+(u,d,s)$-jets	2178.2±11.1	1713.6±10.0	405.6±4.8	75.5±1.9	48.9±1.7	2.4±0.3	0.2±0.1
Total expectation	45908.14±89.9	29208.50±75.1	8745.94±40.9	4395.01±15.8	1768.04±75.1	866.84±8.5	829.90±4.2
Observed Events	45907	28924	8814	4278	1815	879	797

TABLE III: Summary of event yields for the ℓ + 4 or more jets + $\not\!\!E_T$ final states in Run II data. Events in data are compared with the expected number of events in the W/Z+jets samples, in simulated samples of diboson (including WW, WZ, and ZZ processes), $W/Z+b\bar{b}$ or $c\bar{c}$, W/Z+light-quark jets, top quark ("$t\bar{t}$" and "Single top") production, and the multijet background derived from data. All signal yields are for $M_H = 125$ GeV. in this analysis. Uncertainties include only the contribution from statistics. In this channel we use only events with 0 and 1 loose b-tag.

	pre-b-tagging	0 b-tags	1 loose b-tag	1 tight b-tag	2 loose b-tags	2 medium b-tags	2 tight b-tags
$WH\to\ell\nu bb$	1.07±0.02	0.14±< 0.01	0.15±< 0.01	0.24±0.01	0.12±< 0.01	0.13±0.01	0.17±0.01
$ZH\to\ell b\bar{b}+\not\!\!E_T$	0.20±< 0.01	0.02±< 0.01	< 0.01±< 0.01	0.06±< 0.01	0.02±< 0.01	0.01±< 0.01	0.02±< 0.01
$gg\to H\to WW\to\ell\nu jj$	1.01±0.04	0.57±0.03	0.23±0.02	0.08±0.02	0.04±< 0.01	< 0.01±< 0.01	< 0.01±< 0.01
$gg\to H\to ZZ\to\ell\ell jj$	0.01±< 0.01	< 0.01±< 0.01	< 0.01±< 0.01	< 0.01±< 0.01	< 0.01±< 0.01	< 0.01±< 0.01	< 0.01±< 0.01
$VV\to H\to WW\to\ell\nu jj$	1.33±0.02	0.74±0.01	0.34±0.01	0.10±< 0.01	0.07±< 0.01	0.01±< 0.01	< 0.01±< 0.01
$VH\to VWW\to\ell\nu+4j$	2.30±0.06	1.33±0.05	0.54±0.03	0.29±0.02	0.18±0.01	0.01±< 0.01	< 0.01±< 0.01
Diboson	201.25±2.11	112.67±1.65	46.43±1.04	22.45±0.68	13.46±0.52	4.58±0.36	2.10±0.17
$W+b\bar{b}$	298.74±3.33	70.23±1.70	43.68±1.33	91.31±1.85	34.59±1.28	26.53±0.96	20.58±0.81
$Z+b\bar{b}$	41.84±0.43	9.43±0.22	6.49±0.18	12.73±0.25	4.32±0.14	4.30±0.13	3.73±0.12
$W+c\bar{c}$	832.23±7.33	401.10±5.27	204.93±3.70	121.11±2.78	71.31±2.09	21.98±1.16	6.02±0.55
$Z+c\bar{c}$	102.02±1.15	51.84±0.85	25.13±0.59	14.43±0.42	8.99±0.33	2.74±0.18	1.06±0.12
$t\bar{t}$	2813.74±6.07	283.01±1.94	250.44±1.97	659.63±3.05	309.71±2.17	394.20±2.29	512.88±2.52
Single top	60.20±0.49	7.97±0.19	5.96±0.17	16.84±0.28	6.32±0.17	7.94±0.18	9.72±0.19
Multijet	2023.87±30.60	1050.13±24.39	436.01±15.68	225.78±9.48	154.56±8.84	49.51±4.70	41.57±5.84
$W+(u,d,s)$-jets	2804.42±16.47	1932.05±14.63	631.70±7.80	125.66±3.23	124.09±3.41	5.54±0.72	0.78±0.29
$Z+(u,d,s)$-jets	284.73±3.88	210.55±3.42	64.67±1.89	13.78±0.90	10.19±0.67	1.14±0.31	0.04±0.03
Total expectation	9463.04±36.47	4129.02±29.31	1715.46±18.19	1303.73±11.06	737.57±10.07	518.45±5.51	598.50±6.46
Observed Events	9642	3859	1760	1397	817	572	596

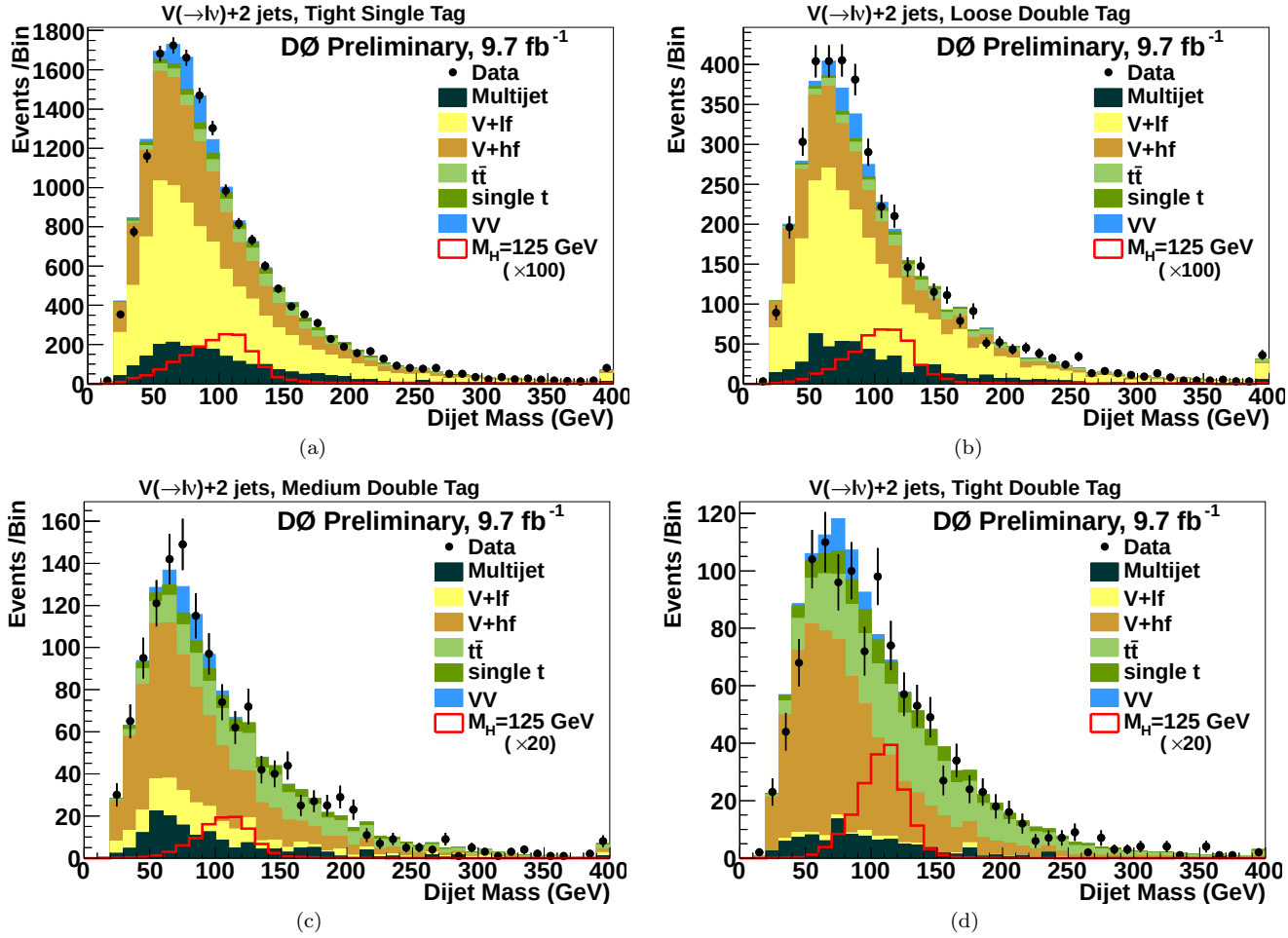

FIG. 3: Dijet mass distribution for all Run II electron and muon channel 2-jet events (a) with one tight b-tag, (b) with two loose b-tags, (c) with two medium b-tags, (d) with two tight b-tags. One b-tag signal events are scaled by a factor of 100; two loose b-tags by 100; two medium b-tags by 20; two tight b-tags by 20. The signal shown is for a Higgs mass of 125 GeV.

VII. SYSTEMATIC UNCERTAINTIES

The systematic uncertainties that affect the signal and backgrounds can be categorized by the nature of their source, i.e., theoretical (e.g., uncertainty on a cross section), modeling (e.g., re-weighting of ALPGEN samples), or experimental (e.g., uncertainty on integrated luminosity). Some of these uncertainties affect only the normalization of the signal or backgrounds, while others also affect the differential distribution of the BDT output.

Theoretical uncertainties include uncertainties on the $t\bar{t}$ and single top-quark production cross sections (7% each [29, 30]), an uncertainty on the diboson production cross section (6% [31]), an uncertainty on W/Z+light-flavor production (6%), and an uncertainty on W+heavy-flavor production (20%, estimated from MCFM). These uncertainties affect only the normalization of these backgrounds.

Uncertainties from modeling that affect the distribution of the BDT output include uncertainties on trigger efficiency as derived from data (3–5%), lepton identification and reconstruction efficiency (5–6%), re-weighting of ALPGEN MC samples (2%), the MLM matching applied to W/Z+light-jet events ($\approx$ 0.5%), and the systematic uncertainties associated with choice of renormalization and factorization scales in ALPGEN as well as the uncertainty on the strong coupling constant (2%). Uncertainties on the ALPGEN renormalization and factorization scales are evaluated by adjusting the nominal scale for each, simultaneously, by a factor of 0.5 and 2.0.

Experimental uncertainties that affect only the normalization of the expected signal and simulated backgrounds arise from the uncertainty on integrated luminosity (6.1%) [44]. Those that affect the BDT distribution include jet taggability (3%), b-tagging efficiency (2.5–3% per heavy quark-jet), the light-quark jet misidentification rate (10%), jet identification efficiency (5%); jet-energy calibration and resolution (varying between 15% and 30%, depending on the process and channel). The multijet background model has a contribution from the statistical uncertainty of data

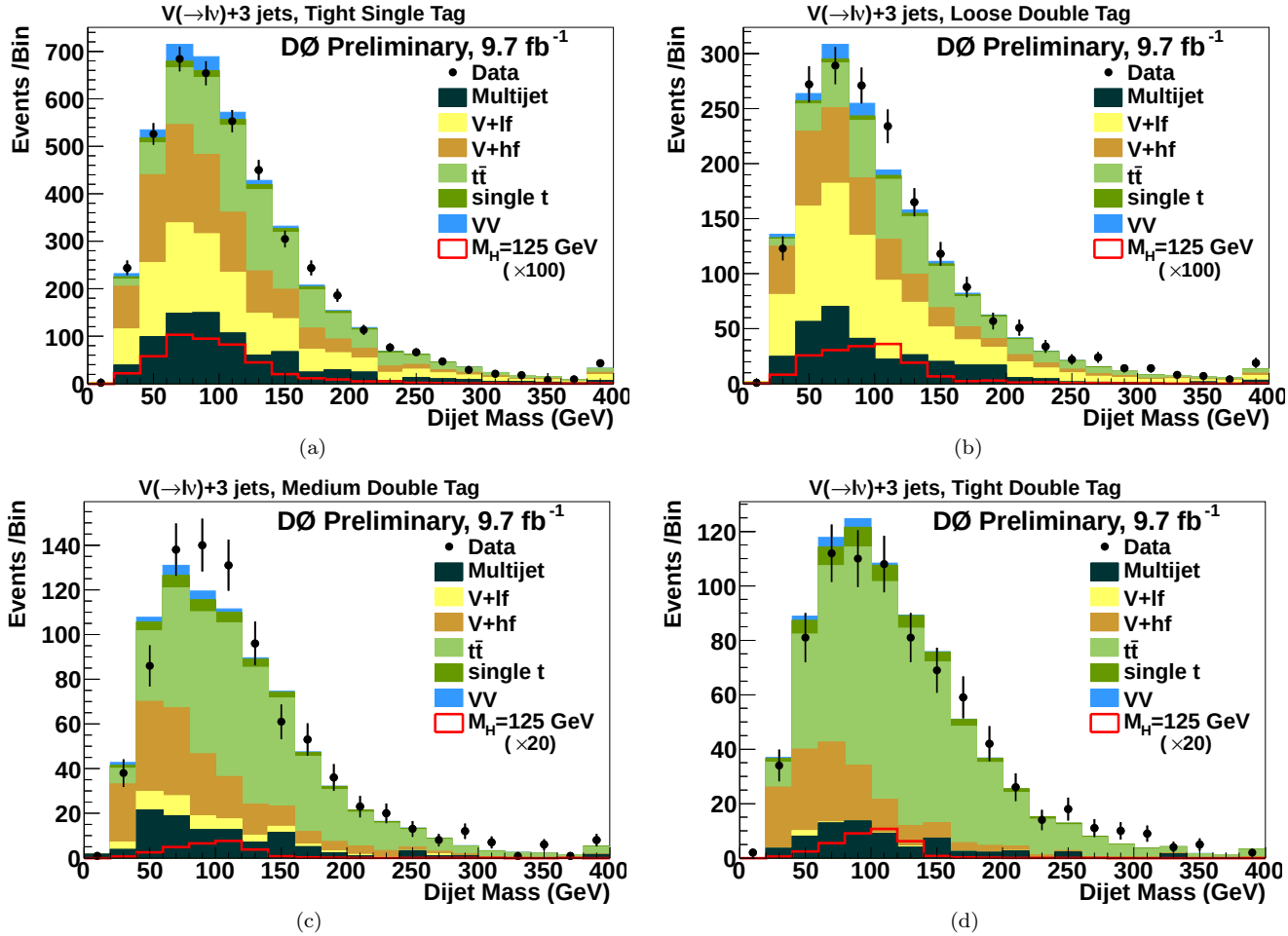

FIG. 4: Dijet mass distribution for all Run II electron and muon channel 3-jet events (a) with one tight b-tag, (b) with two loose b-tags, (c) with two medium b-tags, (d) with two tight b-tags. One b-tag events signal are scaled by a factor of 100; two loose b-tags by 100; two medium b-tags by 20; two tight b-tags by 20. The signal shown is for a Higgs mass of 125 GeV.

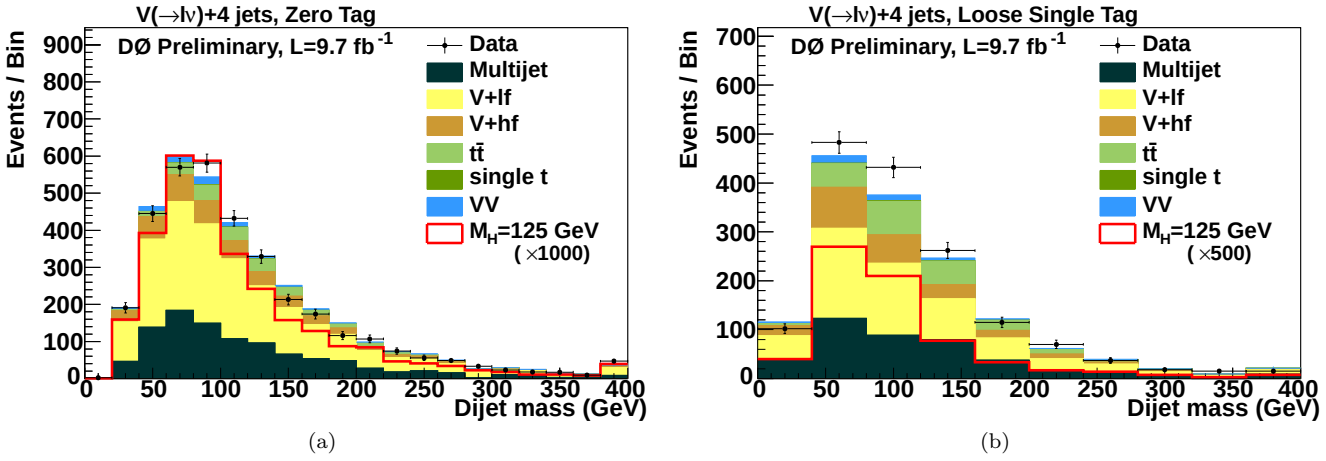

FIG. 5: Dijet mass distribution for all Run II electron and muon channel 4-jet events (a) with zero b-tags, (b) with one loose b-tag. Zero tag signal events are scaled by a factor of 1000; one loose b-tag by 500. The signal shown is for a Higgs mass of 125 GeV.

after tagging (10–20%), which also covers the uncertainty in the flavor dependence of $f_{T|L}$. We do not apply an additional uncertainty on the W+light jets normalization after b-tagging aside from that included in the systematic sources already mentioned.

VIII. RESULTS

We observe no significant excess relative to the SM expectation and proceed to set upper limits on $\sigma(H)$ using BDT discriminants for the different channels. The bins of the BDT distribution are adjusted to assure sufficient Monte Carlo (MC) statistics to protect against bins with zero background expectation. Those bins that do not have sufficient statistics are combined with adjacent bins until the signal and background expectations are large enough that the dominant uncertainty on the predictions is not due to the MC statistics. As described above, each channel is analyzed independently and the limits are then combined. We calculate all limits at 95% C.L. using the modified frequentist CL_s approach with a Poisson log-likelihood ratio as the test statistic [45–47]. We treat systematic uncertainties as "nuisance parameters" constrained by their priors, and the best fits of these parameters are determined at each value of M_H by maximizing the likelihood. We remove the W/Z+jets normalization obtained from the M_W^T and muon $p_T/\not\!\!E_T$ distributions and allow the components to vary by the aforementioned 6% and 20% uncertainties on W+light-flavor and W+heavy-flavor production. Independent fits are performed to the background-only and signal-plus-background hypotheses. All appropriate correlations are maintained among channels and between signal and background. Figure 9 shows the background-subtracted data along with the best-fit $\pm1\sigma$ systematic uncertainties, and the signal contribution for the Run II data set. The log-likelihood ratios for the background-only model and the signal-plus-background model as a function of M_H are shown in Fig. 10(a) for combined 2 and 3 jets events with at least one tight tag, Fig. 10(c) for 4 jets events, and in Fig. 11(a) for the combination. The upper limit at 95% C.L. on the cross section for $\sigma(p\bar{p} \to X + H) \times \mathcal{B}(H \to b\bar{b}$ or $WW)$ for $M_H = 125$ GeV is a factor of 4.5 larger than the SM expectation and our expected sensitivity is 4.1. The same study is performed for all other M_H values between 100 and 200 GeV. The corresponding observed and expected 95% C.L. limits relative to the SM expectation are given in Table IV and in Fig. 10(b) for combined 2 and 3 jets events with at least one tight tag, Fig. 10(d) for 4 jets events, and in Fig. 11(b) for the combination.

TABLE IV: Observed and expected 95% C.L. upper limits on the ratio of $\sigma(p\bar{p} \to X + H) \times \mathcal{B}(H \to b\bar{b}$ or $WW)$ to the SM expectation for each M_H value considered.

M_H (GeV)	90	95	100	105	110	115	120	125	130	135	140	145
Exp. Limit $/\sigma_{SM}$	1.46	1.65	1.88	2.10	2.38	2.70	3.27	4.07	5.29	6.75	8.95	10.86
Obs. Limit $/\sigma_{SM}$	1.20	0.98	1.71	1.83	2.02	2.60	3.60	4.52	4.98	6.90	11.47	11.74
M_H (GeV)	150	155	160	165	170	175	180	185	190	195	200	
Exp. Limit $/\sigma_{SM}$	12.11	14.34	11.85	11.16	12.58	14.31	16.60	21.25	23.92	28.92	30.82	
Obs. Limit $/\sigma_{SM}$	11.24	18.06	10.24	7.98	6.68	14.10	9.94	13.68	21.14	33.01	27.21	

In conclusion, we have performed a search for standard model Higgs production in ℓ+$\not\!\!E_T$+jets final states using two or more jets and b-tagging with the full Tevatron Run II data set of 9.7 fb^{-1} of integrated luminosity from the D0 detector. In events with exactly 2 or 3 jets, only events with one tight or two b-tagged jets are considered in this search. In events with four or more jets, only events with zero or one loose b-tagged jet are considered in this search. The results are in agreement with the expected background, and we set upper limits on $\sigma(p\bar{p} \to X+H) \times \mathcal{B}(H \to b\bar{b}$ or $WW)$ relative to the SM expectations σ(SM) for masses of the Higgs boson between 100 and 200 GeV, as summarized in Table IV and shown in Figure 11. For $M_H = 125$ GeV, the ratio of the observed 95% C.L. limit/(SM) is 4.5 and the expected limit ratio is 4.1.

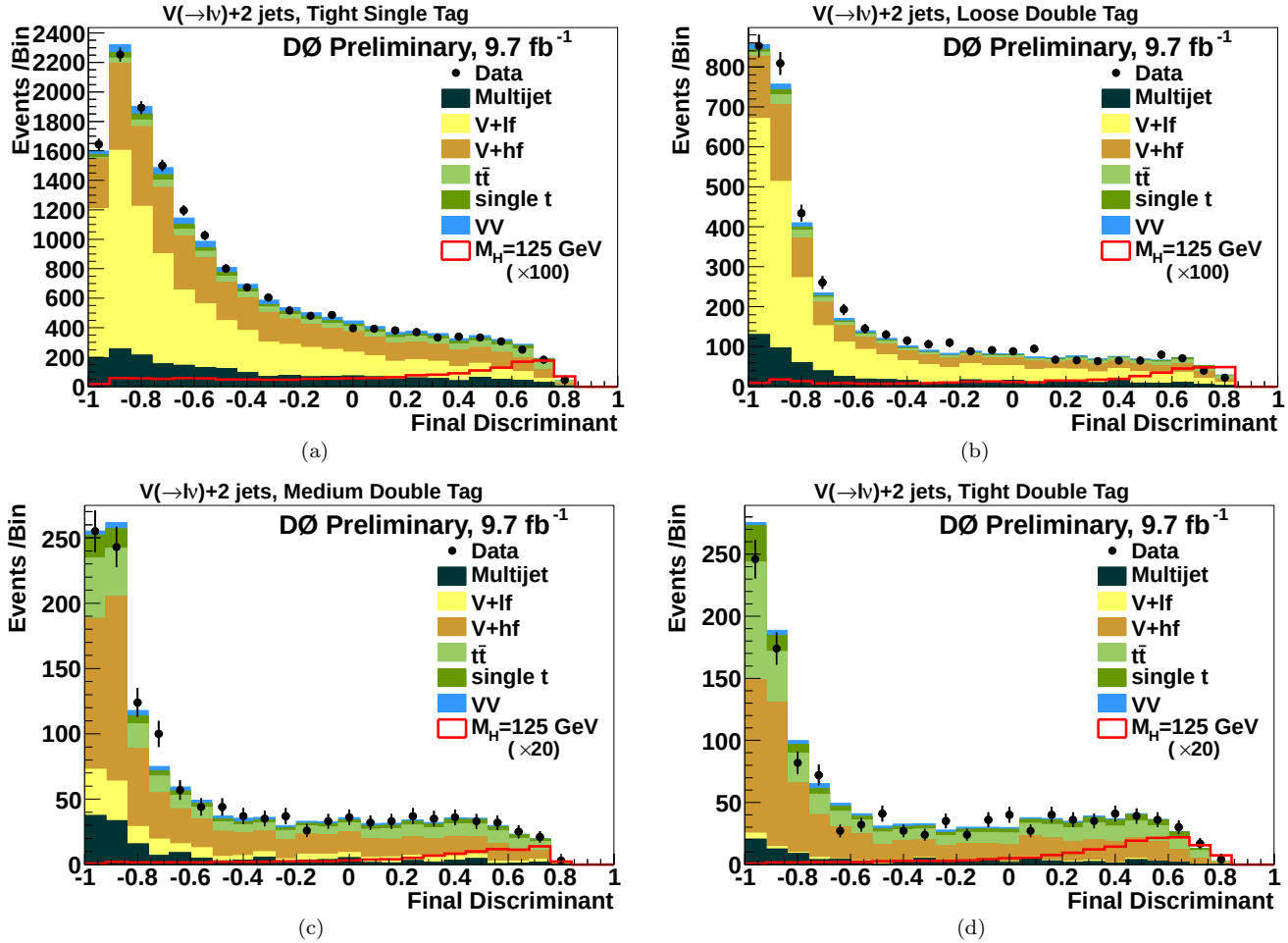

FIG. 6: Higgs signal multivariate discriminant output, for $M_H = 125$ GeV, for Run II events with an electron or muon and two jets with (a) one tight b-tag, (b) two loose b-tags, (c) two medium b-tags, and (d) two tight b-tags, after a fit of all channels to data in the background-only hypothesis. One tight b-tag signal events are scaled by a factor of 100; two loose b-tags by 100; two medium b-tags by 20; two tight b-tags by 20. The signal shown is for a Higgs mass of 125 GeV.

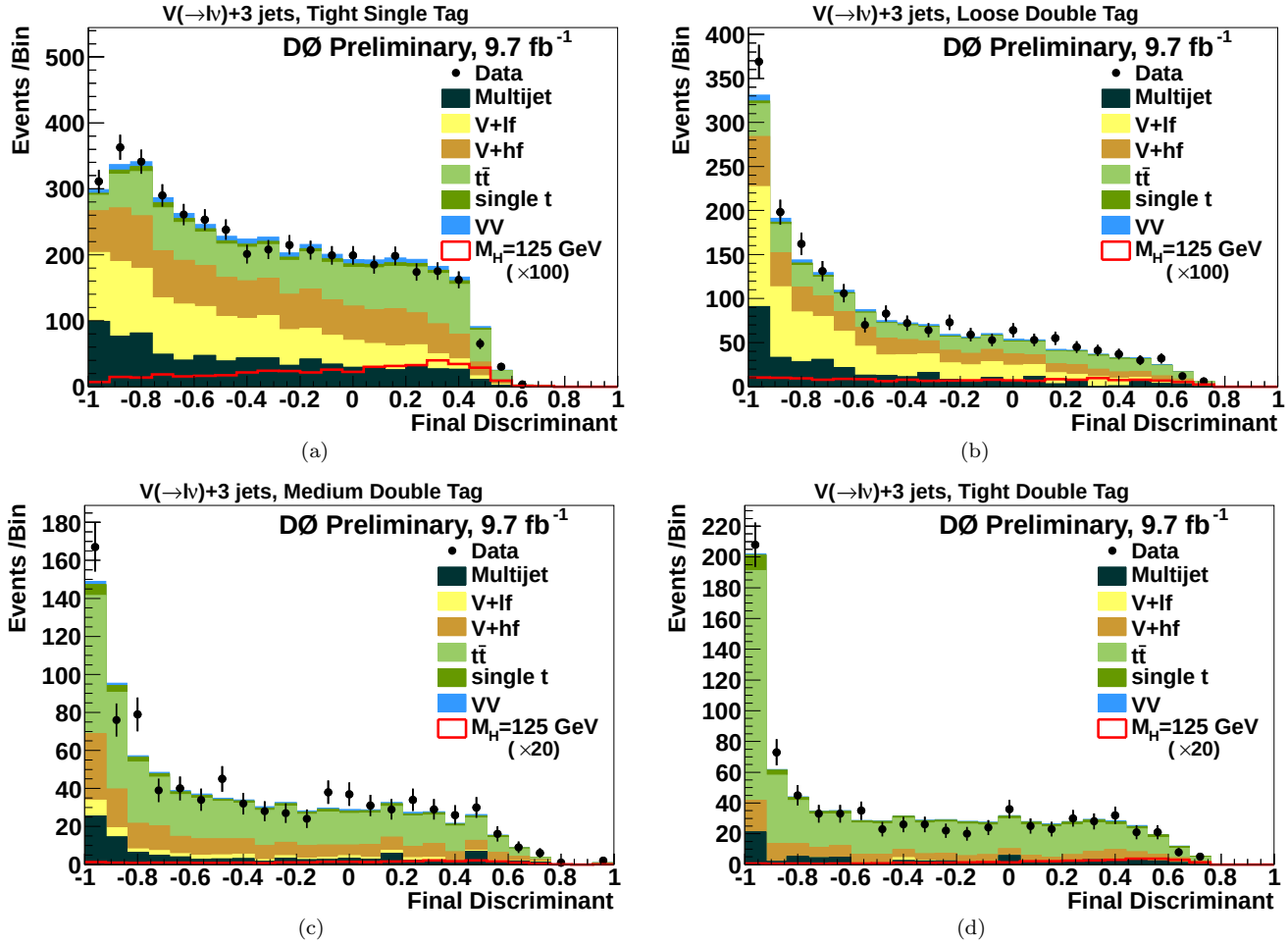

FIG. 7: Higgs signal multivariate discriminant output, for $M_H = 125$ GeV, for Run II events with an electron or muon and three jets with (a) one tight b-tag, (b) two loose b-tags, (c) two medium b-tags, and (d) two tight b-tags, after a fit of all channels to data in the background-only hypothesis. One tight b-tag events are scaled by a factor of 100; two loose b-tags by 100; two medium b-tags by 20; two tight b-tags by 20. The signal shown is for a Higgs mass of 125 GeV.

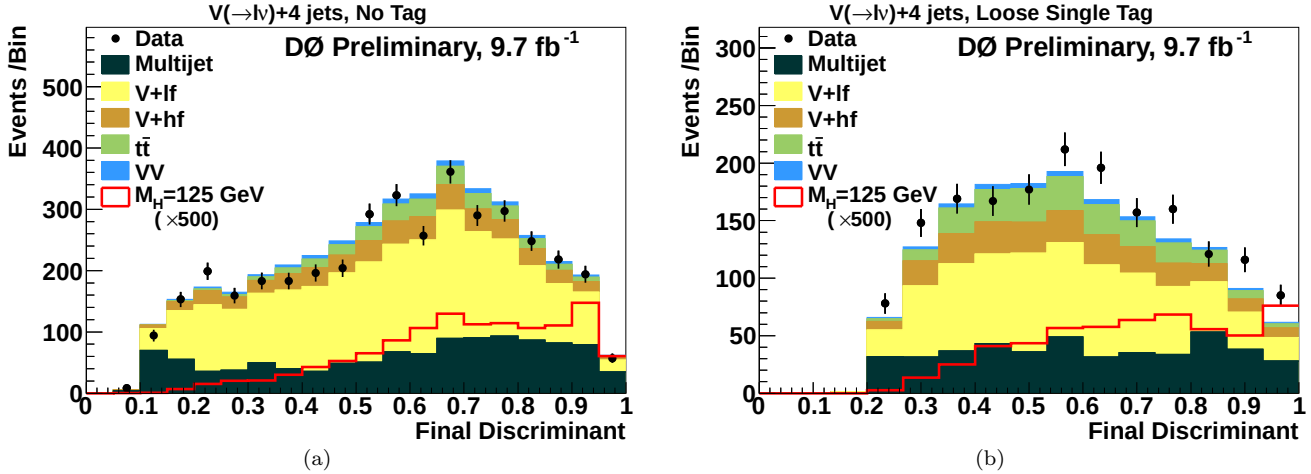

FIG. 8: Higgs signal multivariate discriminant output, for $M_H = 125$ GeV, for Run II events with an electron or muon and at least four jets with (a) zero b-tags and (b) one loose b-tag, after a fit of all channels to data in the background-only hypothesis. Zero tags signal events are scaled by a factor of 500; one loose b-tag by 500. The signal shown is for a Higgs mass of 125 GeV.

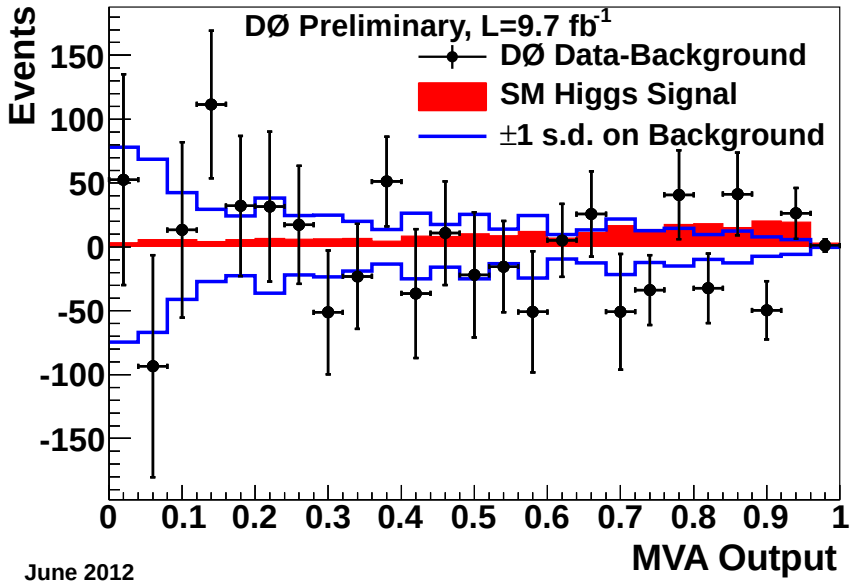

FIG. 9: Distribution in the output of the BDT discriminant for $M_H = 125$ GeV for the difference between data and background expectation, combined for all channels (both e and μ, and 2-jet and 3-jet, all b-tag categories), for the 9.7 fb^{-1} Run II dataset, shown with statistical uncertainties. The solid lines represent the total systematic uncertainty after constraining with data. The darker shaded region represents the SM Higgs signal expectation scaled by a factor of 4.

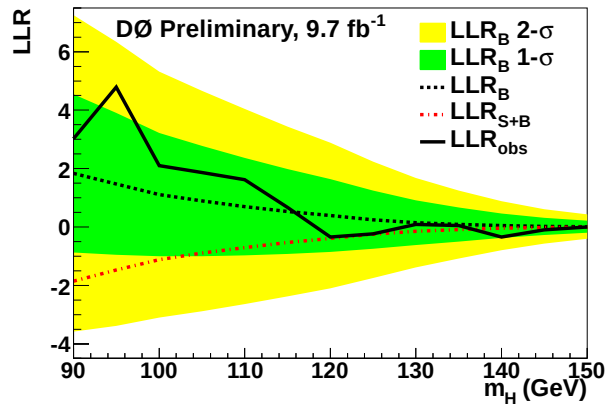

(a)

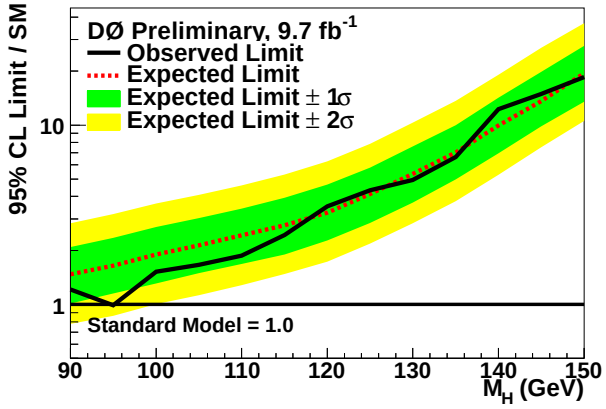

(b)

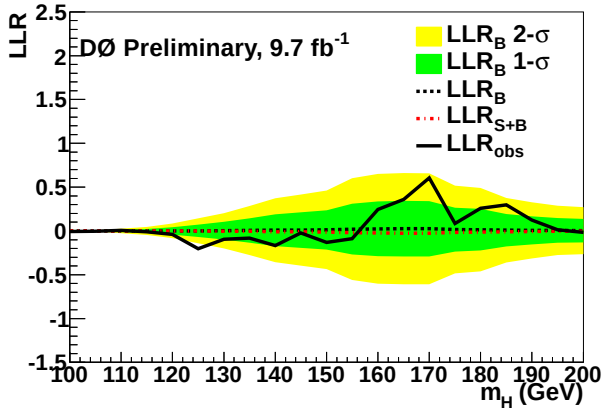

(c)

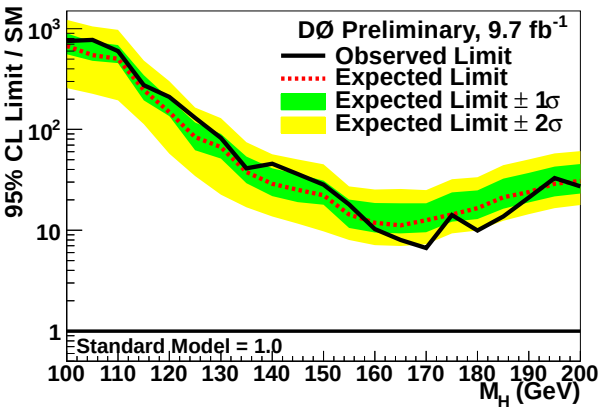

(d)

FIG. 10: Results obtained with the full Run II data set of 9.7 fb^{-1}. Log-likelihood ratio for the background-only model (LLR_B, with 1σ and 2σ uncertainty bands), signal+background model (LLR_{S+B}) and observation in data (LLR_{OBS}) vs. M_H for the (a) 2- and 3-jet one tight b-tag and events with two b-tags and (c) 4-jet zero and one loose b-tag events. The 95% C.L. cross section upper limit (and corresponding expected limit) on $\sigma(p\bar{p} \to X + H) \times \mathcal{B}(H \to b\bar{b}$ or $WW)$ relative to the SM expectation vs. M_H for the same jet multiplicity and b-tagging categories appear in (b) and (d), respectively.

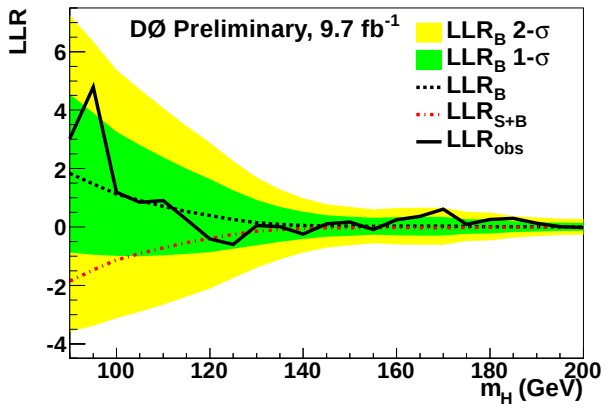

(a)

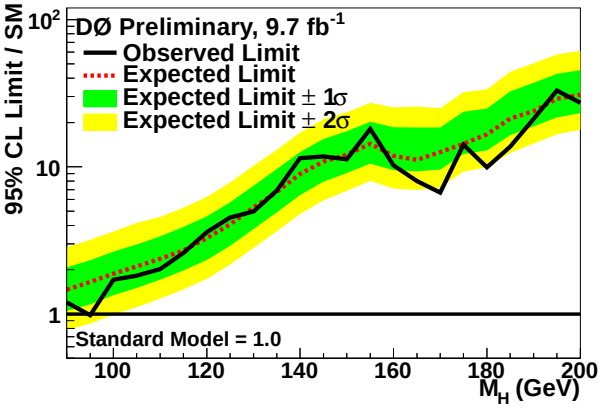

(b)

FIG. 11: Results obtained with the full Run II data set of 9.7 fb^{-1}, using all jet multiplicity and b-tag categories combined. (a) Log-likelihood ratio for the background-only model (LLR_B, with 1σ and 2σ uncertainty bands), signal+background model (LLR_{S+B}) and observation in data (LLR_{OBS}) vs. M_H. (b) The 95% C.L. cross section upper limit (and corresponding expected limit) on $\sigma(p\bar{p} \to X + H) \times \mathcal{B}(H \to b\bar{b}$ or $WW)$ relative to the SM expectation vs. M_H.

IX. ACKNOWLEDGEMENTS

We thank the staffs at Fermilab and collaborating institutions, and acknowledge support from the DOE and NSF (USA); CEA and CNRS/IN2P3 (France); FASI, Rosatom and RFBR (Russia); CNPq, FAPERJ, FAPESP and FUNDUNESP (Brazil); DAE and DST (India); Colciencias (Colombia); CONACyT (Mexico); KRF and KOSEF (Korea); CONICET and UBACyT (Argentina); FOM (The Netherlands); STFC and the Royal Society (United Kingdom); MSMT and GACR (Czech Republic); CRC Program and NSERC (Canada); BMBF and DFG (Germany); SFI (Ireland); The Swedish Research Council (Sweden); and CAS and CNSF (China).

[1] LEP Working Group for Higgs boson searches, R. Barate *et al.*, Phys. Lett. B **565**, 61 (2003).
[2] CDF Collaboration, T. Aaltonen *et al.*, Phys.Rev.Lett. **108**, 151803 (2012).
[3] V. M. Abazov *et al.*, Phys.Rev.Lett. **108**, 151804 (2012).
[4] LEP Electroweak Working Group, Status of July 2011, http://lepewwg.web.cern.ch/LEPEWWG/.
[5] TEVNPH (Tevatron New Phenomena and Higgs Working Group), (2012), arXiv:1203.3774.
[6] ATLAS Collaboration, G. Aad *et al.*, Phys. Lett. B **710**, 49 (2012).
[7] CMS Collaboration, S. Chatrchyan *et al.*, Phys. Lett. B **710**, 26 (2012).
[8] V. M. Abazov *et al.*, Phys. Rev. Lett. **94**, 091802 (2005).
[9] V. Abazov *et al.*, Phys. Lett. B **663**, 26 (2008).
[10] V. M. Abazov *et al.*, Phys. Rev. Lett. **102**, 051803 (2009).
[11] V. M. Abazov *et al.*, Phys. Lett. B **698**, 6 (2011).
[12] V. M. Abazov *et al.*, Phys. Rev. Lett. **106**, 171802 (2011).
[13] V. M. Abazov *et al.*, Submitted to Phys. Rev. D (2012), arXiv:1203.1082.
[14] G. Bernardi *et al.*, Search for Standard model Higgs production in lepton plus jets final states with 9.7 fb^{-1} of Run II data note =.
[15] A. Hocker *et al.*, PoS **ACAT**, 040 (2007), physics/0703039.
[16] V. M. Abazov *et al.*, Nucl. Instrum. Methods Phys. Res. A **565**, 463 (2006).
[17] The pseudorapidity $\eta = -\ln\left[\tan\frac{\theta}{2}\right]$, where θ is the polar angle as measured from the proton beam axis; ϕ is the azimuthal angle. The separation between two objects in η, ϕ space is $\Delta\mathcal{R} = \sqrt{(\Delta\eta)^2 + (\Delta\phi)^2}$.
[18] S. Abachi *et al.*, Nucl. Instrum. Methods Phys. Res. A **338**, 185 (1994).
[19] R. Angstadt *et al.*, Nucl. Instrum. Methods Phys. Res. A **622**, 298 (2010).
[20] M. Abolins *et al.*, Nucl. Instrum. Methods Phys. Res. A **584**, 75 (2008).
[21] H. L. Lai *et al.*, Phys. Rev. D **55**, 1280 (1997).
[22] J. Pumplin *et al.*, J. High Energy Phys. **07**, 012 (2002).
[23] M. L. Mangano, M. Moretti, F. Piccinini, R. Pittau, and A. D. Polosa, J. High Energy Phys. **07**, 001 (2003).
[24] T. Sjostrand, L. Lonnblad, S. Mrenna, and P. Z. Skands, (2003), hep-ph/0308153.
[25] CompHEP, E. Boos *et al.*, Nucl. Instrum. Methods Phys. Res. A **534**, 250 (2004).
[26] E. Boos *et al.*, Phys. Atom. Nucl. **69**, 1317 (2006).
[27] R. Brun and F. Carminati, GEANT Detector Description and Simulation Tool, CERN Program Library Long Writeup W5013, unpublished, 1993.
[28] The Tevatron New Phenomena and Higgs Working Group, CDF Note 10474, 2012.
[29] U. Langenfeld, S. Moch, and P. Uwer, Phys. Rev. D **80**, 054009 (2009).
[30] N. Kidonakis, Phys. Rev. D **74**, 114012 (2006).
[31] J. Campbell and R. Ellis, Phys. Rev. D **60**, 113006 (1999).
[32] J. Campbell, K. Ellis, and C. Williams, MCFM - Monte Carlo for FeMtobarn processes, `http://mcfm.fnal.gov/`.
[33] R. Hamberg *et al.*, Nucl. Phys. B **359**, 343 (1991).
[34] W. van Neerven and E. Zijlstra, Nucl. Phys. B **382**, 11 (1992).
[35] R. Hamberg, T. Matsuura, and W. van Neerven, ZWPROD Program, 1989–2002.
[36] A. D. Martin, R. G. Roberts, W. J. Stirling, and R. S. Thorne, Phys. Lett. B **604**, 61 (2004).
[37] J. Campbell, (2001), hep-ph/0105226.
[38] V. M. Abazov *et al.*, Phys. Rev. Lett. **101**, 062001 (2008).
[39] V. M. Abazov *et al.*, Phys. Rev. Lett. **102**, 251801 (2009).
[40] TMVA package, http://tmva.sourceforge.net/.
[41] G. C. Blazey *et al.*, (2000), hep-ex/0005012.
[42] J. Alwall *et al.*, Eur. Phys. J. C **53**, 473 (2008).
[43] V. M. Abazov *et al.*, Nucl. Instrum. Methods Phys. Res. A **620**, 490 (2010).
[44] T. Andeen *et al.*, (2007), FERMILAB-TM-2365.
[45] T. Junk, Nucl. Instrum. Methods Phys. Res. A **434**, 435 (1999).
[46] A. L. Read, J. Phys. G **28**, 2693 (2002).
[47] W. Fisher, (2007), FERMILAB-TM-2386-E.

[48] S. J. Parke and S. Veseli, Phys. Rev. **D60**, 093003 (1999), hep-ph/9903231.

APPENDIX A: MULTIVARIATE DISCRIMINANT INPUTS

TABLE V: Table of multivariate discriminant input variables for the specialized signal vs. multijet (MVAQCD) discriminant.

Variable	Definition
η_ν	The neutrino pseudorapidity, calculated by choosing the smaller absolute value of the 2 neutrino longitudinal momentum solutions, assuming the electron and $\not\!\!E_T$ are the products of an on-shell W decay
$\not\!\!E_{T\,sig}$	The missing-E_T significance: likelihood that the $\not\!\!E_T$ arises from physical sources
$\Delta\eta(\nu,\ell)$	$\Delta\eta$ between the charged lepton and neutrino (neutrino η calculated as above)
Max $\Delta\eta(\ell,j)$	The maximum $\Delta\eta$ between the charged lepton and any jet
W twist	$\tan^{-1}(\frac{\Delta\phi(\nu,e)}{\Delta\eta(\nu,e)})$ (neutrino η calculated as above)
$\cos\theta_\ell$	Cosine of the lepton polar angle in the (ℓ,ν) center of mass system
Σ^H_{min}	$\frac{\Delta R(j_1,j_2)\cdot p_T^{j,max}}{\sum p_T^j}$ where $p_T^{j,max}$ corresponds to the highest jet p_T
Higgs decay product velocity	$-log\left(1-\sqrt{(1-4\sqrt{(m_1+m_2)/m)}}\right)$ where m_1, m_2, and m are respectively the leading, sub-leading and di-jet invariant mass
WH asymmetry	Mass asymmetry between W and H candidates: $(m_W - m_{bb})/(m_W + m_{bb})$
$\not\!\!E_T$	Missing transverse energy
H_T	Scalar sum of the lepton, neutrino candidate and selected jets p_T
Centrality	$\frac{\sum_i p_T^i}{\sum_i \lvert\vec{p_i}\rvert}$ where i runs over the jets and lepton

TABLE VI: Table of multivariate discriminant input variables for the final signal discriminant in $WH \to \ell\nu bb$ focused channels, including the 2-jet and 3-jet exclusive final states with one tight b-tagged jet or two b-tagged jets. Variables noted with a (†) are only used in events with one tight b-tagged jet or two loose b-tagged jets, while variables noted with a (‡) are only used in events with two medium b-tagged jets or two tight b-tagged jets.

Variable	Definition
b-ID output	summed b-tagging algorithm outputs for leading and sub-leading jets
m_{bb}	invariant mass formed by the pair of jets with the highest b-tagging algorithm output values
H decay product velocity	$-log\left(1-\sqrt{1-4\sqrt{(m_1+m_2)/m}}\right)$ where m_1, m_2, and m are respectively the leading, sub-leading and di-jet invariant masses
$q_\ell \times \eta_\ell$	lepton charge times pseudorapidity
$\Delta\eta_{max}(j,\ell)$	the maximum $\Delta\eta$ between any jet and the lepton
Σ_{min}	$\frac{\Delta R(j_1,j_2)\times p_T^{j,min}}{\sum p_T^j}$, where $p_T^{j,min}$ corresponds to the smallest jet transverse momentum
$(\vec{p_T^\ell}+\vec{\not{E}_T})/(p_T^\ell+\not{E}_T)$	vector sum of the lepton p_T and $\not{E}_T$ over their scalar sum
$q^\ell \times \eta_{j_1}$	lepton charge times the leading jet pseudorapidity
$m_{\ell\nu j2}$	invariant mass of lepton, neutrino and second leading jet
Centrality	$\frac{\sum_i p_T^i}{\sum_i \lvert\vec{p_i}\rvert}$ where i runs over the jets and lepton
Aplanarity †	$3\lambda_3/2$ where λ_3 is the smallest eigenvalue of the normalized momentum tensor $S^{\alpha\beta}=\frac{\sum_i p_i^\alpha p_i^\beta}{\sum_i \lvert\vec{p_i}\rvert^2}$, where $\alpha,\beta=1,2,3$ correspond to the x,y,z momentum components and i runs over the jets and lepton
WH asymmetry †	Mass asymmetry between W and H candidates: $(m_W-m_{bb})/(m_W+m_{bb})$
p_T^{j2} †	second leading jet p_T
MVAQCD ‡	Signal vs. multijet background focused multivariate discriminant output
$cos(\theta^*)$ ‡	Cosine of angle between W candidate and u-quark in zero-momentum frame [48]
$cos(\chi^*)$ ‡	Cosine of angle between charged lepton and spin-basis rotated dijet system in W rest frame [48]
$m_T^{j_1 j_2}$ ‡	Transverse mass of leading and second leading jets
$\Delta\mathcal{R}(\ell,j_1)$ ‡	Separation between leading jet and charged lepton in (η,ϕ) space [17]
$\Sigma(p_T)$ ‡	Scalar sum of transverse momentum of charged lepton, neutrino, and all jets

TABLE VII: Table of multivariate discriminant input variables for the final signal discriminant in $VH \to \ell\nu jjjj$ focused channels, including the final states with 4 or more jets and zero or one loose b-tagged jet.

Variable	Definition
$\Delta\eta(\ell,\nu)$	$\Delta\eta$ between the charged lepton and the neutrino
$\Sigma p_T(\ell, \not{E}_T)$	Sum of charged lepton p_T and the missing transverse energy
$m_{\ell\nu j_1 j_2}$	Invariant mass of lepton, neutrino and first and second leading jets
$\Delta\eta(\nu, j_3)$	$\Delta\eta$ between third leading jet and neutrino
$\cos\theta(\ell,\nu)_{CM}$	$\cos\theta$ between lepton and neutrino in $\ell\nu j_1 j_2$ center of mass frame
$\Delta\eta(\ell, W)$	$\Delta\eta$ between lepton and W
M_W^T	W boson transverse mass
Max $\Delta\eta(\ell, j)$	The maximum $\Delta\eta$ between the charged lepton and any jet
Σ_ℓ	$\frac{\Sigma_i \Delta R(j_i,\ell)\times p_T^{j_i}}{\sum p_T^j}$, where p_T^ℓ is the charged lepton transverse momentum
E_ℓ	Charged lepton energy
$\theta_{\ell\nu}$	Angle between the charged lepton and neutrino candidate
W recoil	p_T of the W with respect to the thrust vector
W twist	$\tan^{-1}(\frac{\Delta\phi(\nu,e)}{\Delta\eta(\nu,e)})$ (neutrino η calculated as above)
η_ν	Neutrino candidate η (after constraining p_z^ν to fit the W mass)
$m_T^{\ell\nu jjjj}$	Transverse mass of the $\ell\nu jjjj$ system
θ_{jj}^{CM}	Angle between Higgs decay jets in the center of mass frame for semileptonic Higgs candidates ($H \to \ell\nu jj$)
$\Sigma p_T(\ell, \not{E}_T, j_{1234})$	Sum of charged lepton p_T, missing transverse energy and p_T of leading four jets
$cos(\theta(j_1,\ell))$	Cosine of the angle between the highest p_T Higgs decay jet and the charged lepton in the center of mass frame for semileptonic Higgs candidates ($H \to \ell\nu jj$)
E_{j1}/E_{j2} (Jet Pair 1; CM)	Energy ratio between jets from one hadronic W decay for fully hadronic Higgs candidates ($H \to jjjj$)
E_{j1}/E_{j2} (Jet Pair 2; CM)	Energy ratio between jets from second hadronic W decay for fully hadronic Higgs candidates ($H \to jjjj$)
Sphericity	$3\lambda_2/2$ where λ_2 is the second highest eigenvalue of the normalized momentum tensor $S^{\alpha\beta} = \frac{\sum_i p_i^\alpha p_i^\beta}{\sum_i \lvert\vec{p_i}\rvert^2}$, where $\alpha,\beta = 1,2,3$ correspond to the x,y,z momentum components and i runs over the jets and lepton
Scaled $\not{E}_T$	$\sum_{n=0}^{numJets} (\sqrt{jetE(n)} \times \sin jet\theta(n) \times \cos\Delta\phi[jet(n), \not{E}_T])^2$
$(p_T^\ell + \not{E}_T)/(p_T^{j1} + p_T^{j2})$	Ratio of the sum of the charged lepton and neutrino p_T to the sum of the p_T of the first two leading jets

APPENDIX B: COMPARISON OF CURRENT RESULTS TO MARCH, 2012 RESULTS

The major changes to this analysis since March, 2012 [14], include:

- The 4-jet inclusive search channels, using electron and muon events with zero b-tagged jets and one loose b-tagged jet, were added to the original 2-jet and 3-jet b-tagged channels.
- Muon subdetector acceptance has been extended from $|\eta| < 1.6$ to $|\eta| < 2.0$.
- In the muon channel we have lowered the upper muon p_T cut from 300 GeV to 150 GeV and added an upper W transverse mass cut of 180 GeV to suppress backgrounds from events with poorly measured muon tracks. The signal loss is 1.5%.
- We now require that the second leading jet in the event have $p_T > 23$ GeV if the jet is within $0.8 < |\eta| < 1.4$ as this region of the calorimeter has worse resolution. The signal loss is $< 1\%$.
- Events with two b-tagged jets were divided into two subcategories (loose and tight) in March, 2012, and are now divided into three subcategories (loose, medium, and tight).
- The multijet background estimation has been updated to improve modeling of the instrumental background.
- Variables sensitive to the spin correlation between Higgs boson decay products have been added to the list of final discriminant variables for the 2-jet and 3-jet channels.
- The final multivariate discriminants were trained and evaluated on the fully combined sample of Run II data, instead of training and evaluating separately for different subsets of data based on when events were recorded.
- Due to merging all Run II data when evaluating the final multivariate discriminant, a finer binning of the final MVA output is used to evaluate the limits.

The results from this updated analysis are compared to the results from the March, 2012, analysis in Figs. 12–15. Since this analysis combines multiple channels into the final result, including multiple b-tagging categories in each considered jet multiplicity, it is useful to collect information from all channels into a single distribution to facilitate comparison to the previous result. Individual bins of final MVA output from all channels are reordered by their signal to background ratio (s/b) and bins with similar s/b are combined. The highest s/b bins from this analysis and the March, 2012, analysis are shown in Fig. 12. Figure 13 shows the same distribution, but with contributions from background subtracted. Figure 14 shows the cumulative integral of the distribution from Fig. 12, starting from the highest s/b bin. For a given amount of accumulated events, the number of integrated signal events is higher in the updated analysis, demonstrating the improved sensitivity. Finally, Fig. 15 shows a direct comparison between the expected and observed limits from this analysis and the March, 2012, result.

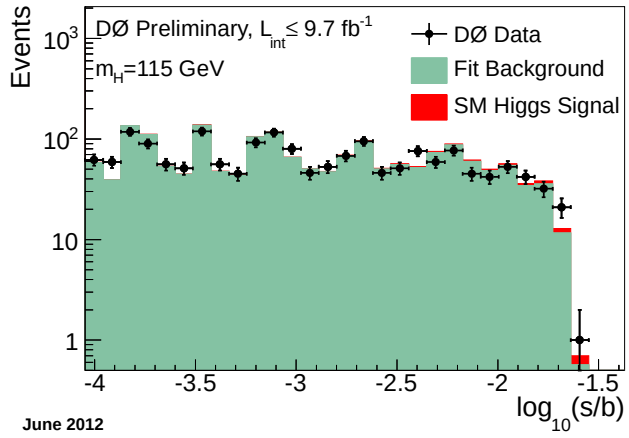

(a)

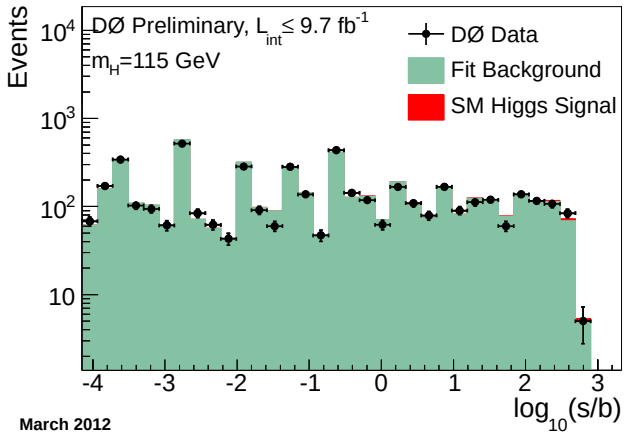

(b)

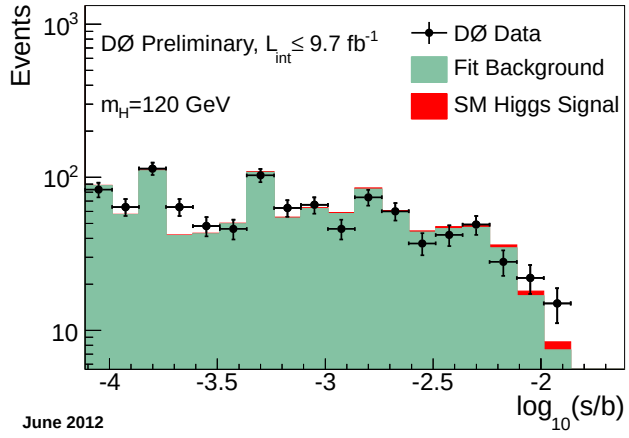

(c)

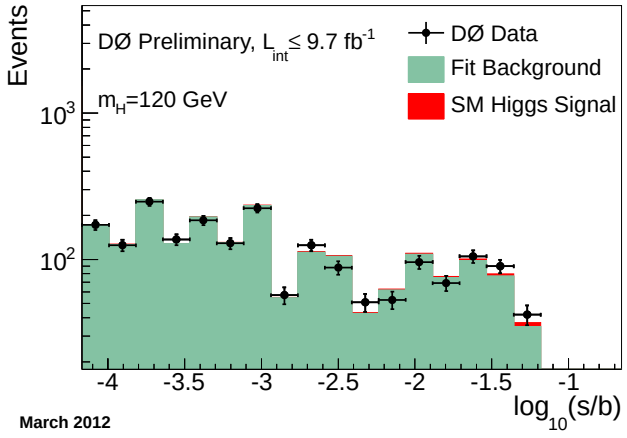

(d)

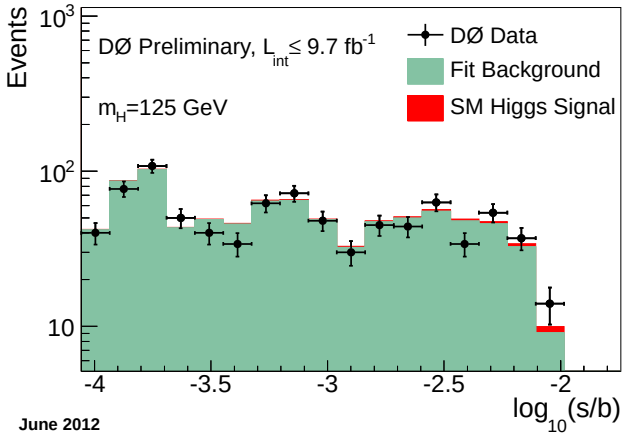

(e)

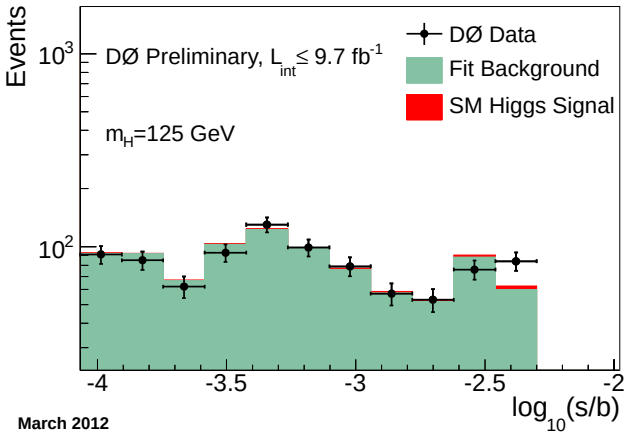

(f)

FIG. 12: Distributions of $log_{10}(s/b)$, for the data from the current $WH \to \ell\nu bb$ result [(a), (c) and (e)] and the March, 2012, $WH \to \ell\nu bb$ result [14] [(b), (d) and (f)] for Higgs boson masses of 115, 120, and 125 GeV/c^2, respectively. The data are shown with points, and the expected signal is shown stacked on top of the backgrounds, which have been fit to the data within their systematic uncertainties. Underflows and overflows are collected into the leftmost and rightmost bins.

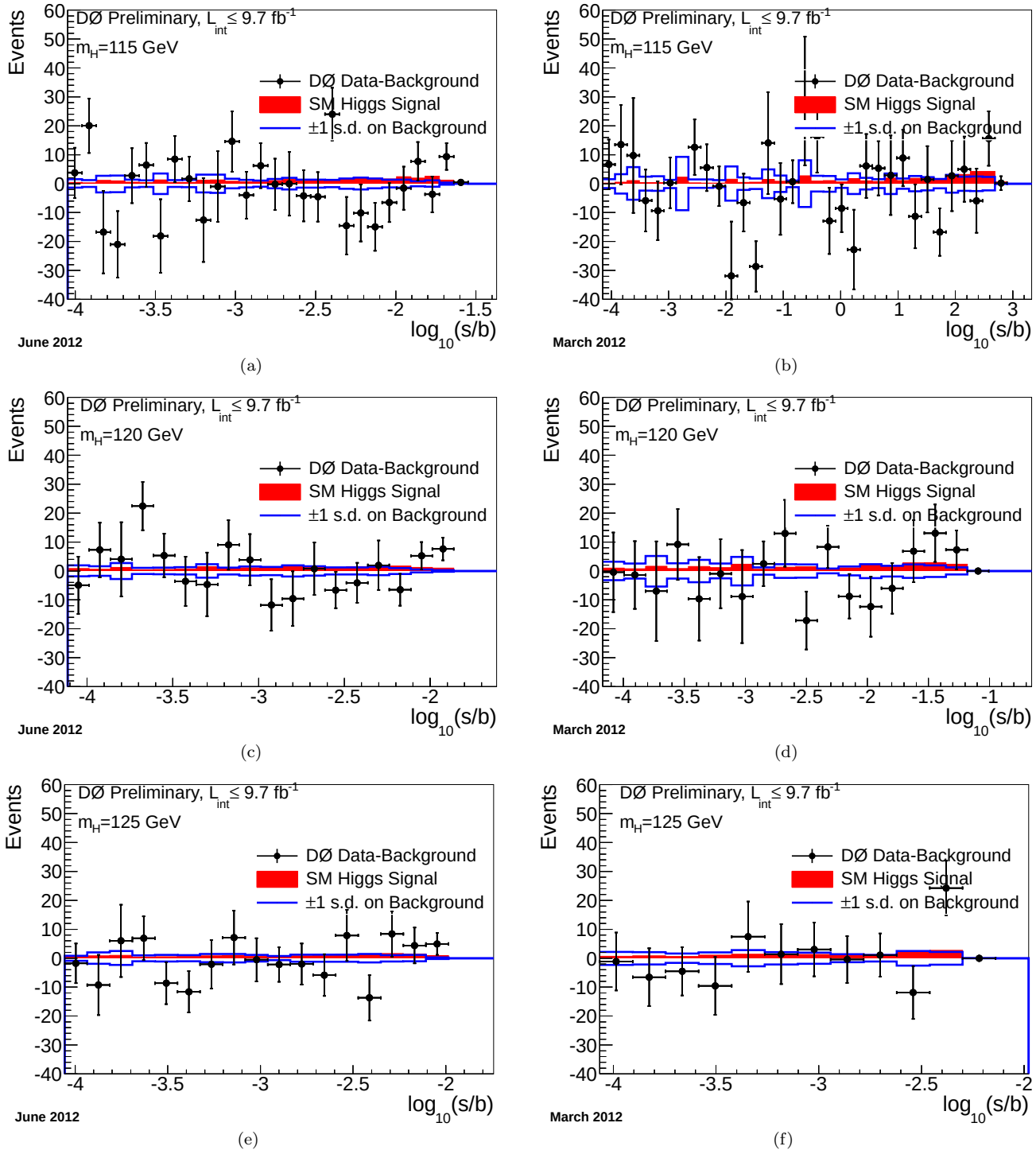

FIG. 13: Distribution in the output of the BDT discriminant for the difference between data and background expectation, shown with statistical uncertainties, for the current $WH \to \ell\nu bb$ result [(a), (c) and (e)] and the March, 2012, $WH \to \ell\nu bb$ result [14] [(b), (d) and (f)] for Higgs boson masses of 115, 120, and 125 GeV/c^2, respectively. The solid lines represent the total systematic uncertainty after constraining with data. The darker shaded region represents the SM Higgs signal expectation.

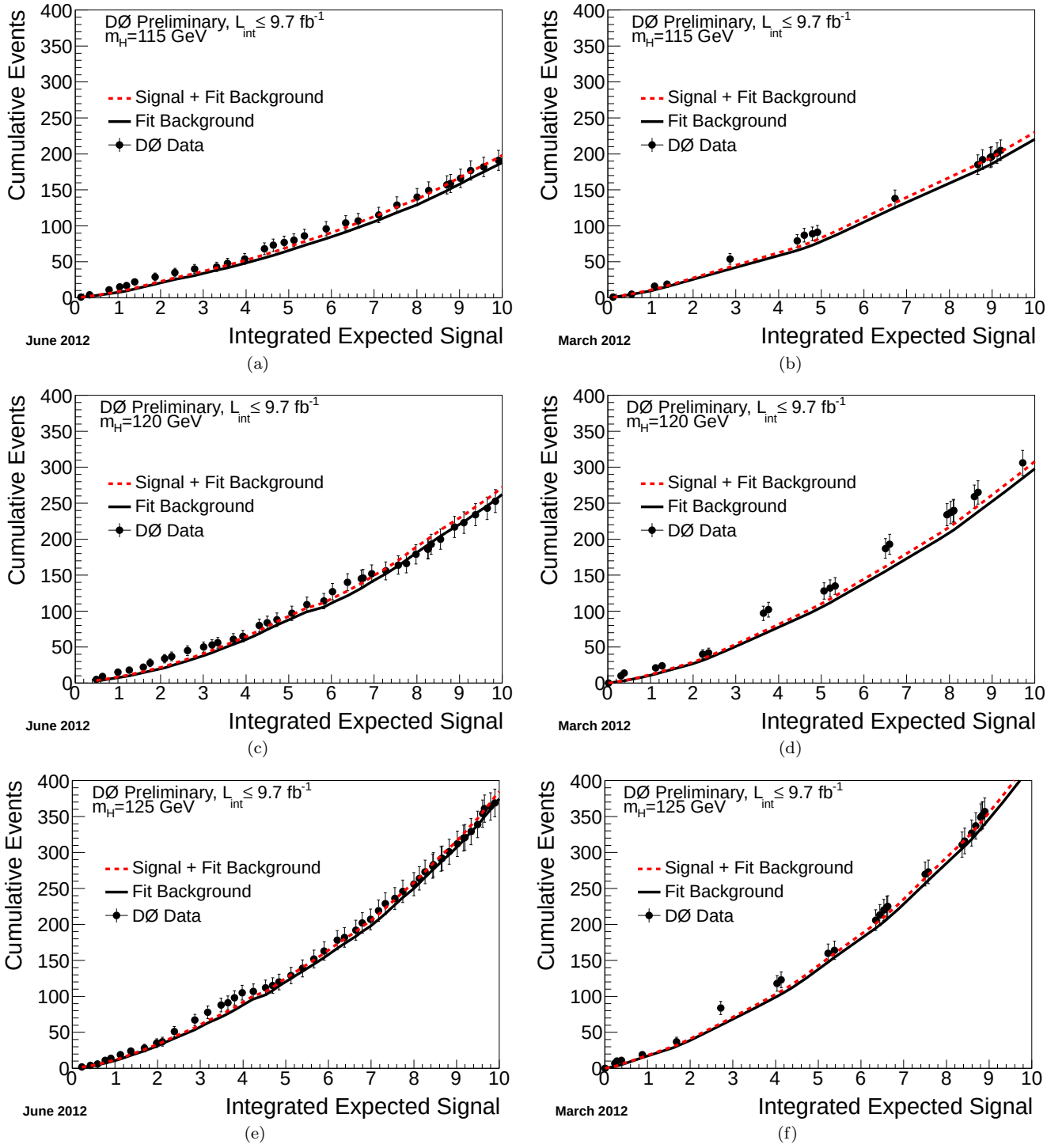

FIG. 14: Integrated distributions of MVA output as ordered by s/b (see Fig. 12), starting at the high s/b side, for the current $WH \to \ell\nu bb$ result [(a), (c) and (e)] and the March, 2012, $WH \to \ell\nu bb$ result [14] [(b), (d) and (f)] for Higgs boson masses of 115, 120, and 125 GeV/c^2, respectively. The total signal+background and background-only integrals are shown separately, along with the data sums. Data are only shown for bins that have data events in them.

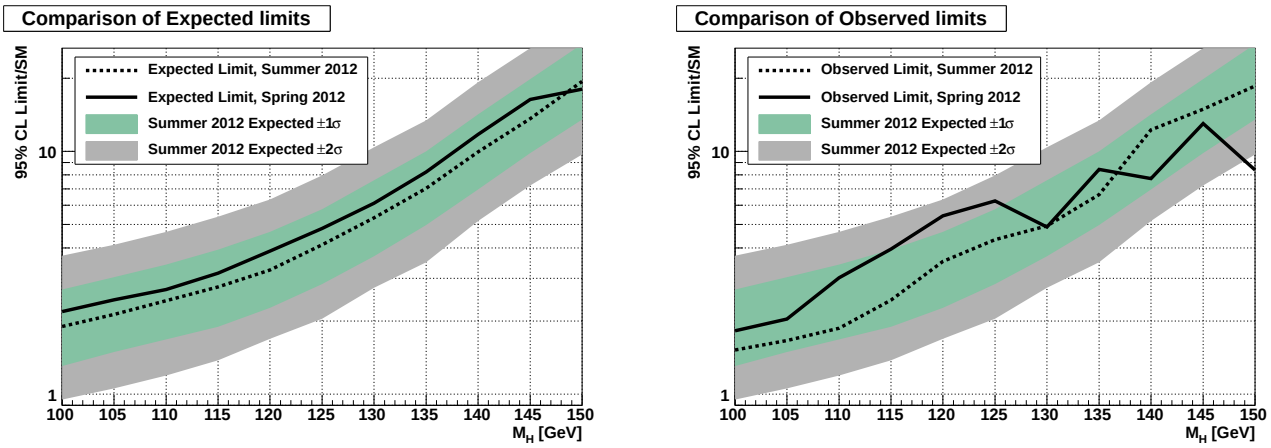

(a) (b)

FIG. 15: Comparison of (a) the expected limit and (b) the observed limit for the current $WH \to \ell\nu bb$ result and the March, 2012, $WH \to \ell\nu bb$ result [14]. In each plot, the current result is shown as a dashed line and the March, 2012, result is shown as a solid line. The colored bands indicate the 1σ and 2σ uncertainty bands on the expected limit for the current result.